Derivation of exact results for the single-ion Kondo problem with the use of diagrammatic methods

S. E. Barnes
Department of Physics, University of Miami, Coral Gables, Florida 33124
(Received 12 March 1985)

It is shown that exact results for the single-impurity Kondo problem can be obtained by diagrammatic methods. The results for the susceptibility and specific heat agree with those obtained by Wilson's numerical methods. In particular, the crossover $W'=(\pi/e)^{1/2}$ and Wilson $R=2$ ratios are reproduced exactly. Conduction-electron scattering from the impurity reaches the unitarity limit corresponding to a phase shift $\delta=\pi/2$. Both this and the compensation of the impurity spin are also exact results. The methods described are relatively easily extended to the Anderson model and the corresponding lattice problems.

I. INTRODUCTION

Probably because of recent work on the intermediate-valence systems and heavy-fermion superconductors there has been a considerable reawakening of interest in the Kondo problem, particularly in the lattice versions of both the s-d exchange and Anderson Hamiltonians. At the level of the single-impurity problem there exists the exact solution by Wilson,[1] the details of which confirmed by and large the solution "in principle" obtained earlier by Anderson and co-workers.[2] However, both this and the recent Bethe-ansatz methods[3] are of little help for the lattice problems either because of the computational difficulties or, in the case of the Bethe methods, their intrinsic nature. Diagram methods, once condemned as "wilderness methods," have again become popular.[4] Such methods, if they could be made tractable, have the advantage of being easily generalized to the lattice problems. Some progress has recently been made in this direction. However, it still seems to remain the opinion of most workers that the crossover from the weak- to strong-coupling limits of the problem cannot be described by these methods.

The purpose of this paper is to describe in detail diagram methods which yield exact results[1,3] for the single-impurity Kondo problem. In particular, the method reproduces the value $W'=(\pi/e)^{1/2}$ for the ratio of the high-field, weak-coupling scale temperature T_H to low-field, strong-coupling scale T_0. The precise definitions are given in later sections. Also given exactly is $R=(\Delta\chi/\chi)/(\Delta C_v/C_v)=2$, the Wilson ratio of the change in the susceptibility to that in the specific heat, both normalized to the free-electron values.

As has been emphasized in connection with the Anderson model,[5] these results cannot be obtained without explicitly considering certain vertex corrections. The high degeneracy limit has been suggested[5] as a way of avoiding such corrections. Methods which also use the author's Abrikosov method for the Anderson model[6] are an alternative. These methods permit the systematic evaluation of vertex corrections. It was possible to show for the $U=0$ limit of this model that the vertex corrections and self-energies beyond fourth order cancel exactly, permitting the solution of this admittedly trivial limit.[7] The method, however, has quite general applicability. It does not directly involve Ward identities, but rather, treats the single-particle self-energies, i.e., those associated with the individual propagators, on the same footing as the vertex corrections. Both contribute to what can, in a real sense, be called two-particle self-energies. These methods were evolved from Holstein's work[8] on transport in the electron-phonon system and were first used by Barnes and Zitkova-Wilcox[9] in the derivation of spin transport equations for electron-spin resonance (ESR) in dilute magnetic alloys over a decade ago. The equivalent of the vertex corrections considered by Coleman[5] *are* included in the present work. Other important vertex corrections of the general structure of those shown in Fig. 1(a) are also accounted for. It can be shown that the totality of these corrections, for an isotropic exchange, cancel either against each other or against omitted dressings.

The approach involves the evaluation of a certain two-particle self-energy Σ for the impurity transverse dynamic susceptibility. In the weak-coupling limit, this is associated with the energy required to suddenly flip the impurity spin. In the strong coupling it evolves into the energy separation between the singlet ground state and an excited (triplet) state of the impurity; it has a value $\sim T_0$ and acts as an infrared cutoff in the logarithmic integrals of the theory. These integrals will be denoted I, and in the large field limit $I\sim\ln(H/D)$ as usual. Because the self-energy acts as a cutoff, it follows that in the small field limit the leading order $(\rho J)^n I^{n-1}\sim\rho J$, regardless of the power n, and that the next to leading order and, so on, are small by increasing powers of ρJ. Thus in the scaling limit, $\rho J\to 0, D\to\infty$ with T_0 a constant, only the self-consistently evaluated parquet, or leading order, approximation is required.

The present approach differs from the well-accepted methods of Abrikosov and Migdal.[10] Their scaling equation in the present notation would be

$$\frac{dg}{dy}=2g^2(1+g)+\cdots\ , \tag{1.1a}$$

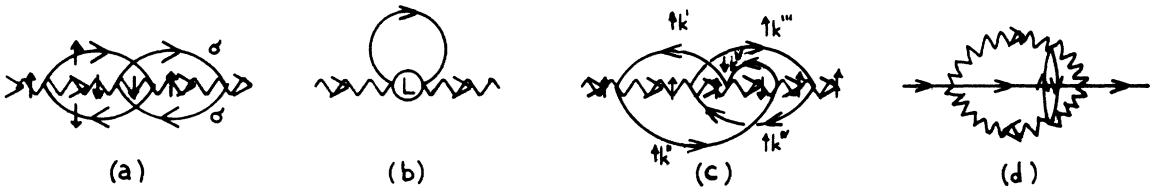

FIG. 1. (a) Overlapping bubble type of vertex correction. These are required in the next to leading logarithmic approximation. (b) The renormalized $O(J)$ longitudinal vertex. Only this vertex will eventually be required. (c) This vertex correction which contains transverse vertices within a longitudinal bubble is a dressing of a purely longitudinal diagram. (d) This type of vertex correction of a conduction-electron self-energy is included. The diagram conventions are described in Fig. 2 and the text.

where g is the renormalized, or effective, exchange scattering strength near the Fermi surface, $y=\ln(\varepsilon/D)$ is the logarithmic integral, and the right-hand side is intended to be a power series in g. The coefficient of $O(g^4)$ is also known.[10] The quantity g is the "invariant charge" in this formulation and is taken to be real. Integrating gives

$$\tfrac{1}{2}(1/g+\lg+\cdots)=\ln(\varepsilon/T_K)\ , \tag{1.1b}$$

where again the ellipsis represents omitted terms.

However, as discussed at length by Tsvelick and Wiegman,[3] the invariant charge is not unique. The choice made in the present work corresponds to a scaling equation:

$$\frac{dg}{dy}=2g^2/(1-g)\ , \tag{1.2a}$$

which when integrated gives exactly

$$\tfrac{1}{2}(1/g+\lg)=\ln(Z/T_K)\ . \tag{1.2b}$$

In this equation g, related to the true renormalized exchange matrix element, is complex and defined differently (see below). Also, the cutoff which was the energy ε has been replaced by an effective such quantity:

$$Z=\Sigma-h\ ,$$

where h is the Zeeman energy and Σ is the two-particle self-energy discussed above. (In the body of the text T_K is replaced by K; the former is reserved for Wilson's definition of the Kondo temperature.)

Different choices for the "invariant charge" lead not only to different scaling equations but also to different expansions for the various physical quantities. Their choice might be thought of as "bad." It is suggested that the present choice of the invariant charge plus the self-consistent nature of the cutoff Z is the optimal one. Not only does it lead to a simple scaling equation which can be readily integrated, but also, and this is most important, physical quantities like the susceptibility have easy to handle expansions in terms of the invariant charge in *both* the weak- and strong-coupling limits. It is perhaps worth emphasizing that all of the diagram structures explicitly considered by those authors *are* included here.

The physics involved in the choice of invariant charge is perhaps best understood in terms of the simple spin-dependent potential scattering Hamiltonian:

$$H=\sum_k \varepsilon_{k\sigma}n_{k\sigma}+g\mu_B HS_z-(J/N)S_z s_z(\mathbf{R}=0)\ , \tag{1.3}$$

where $s_z(\mathbf{R}=0)$ denotes the z component of conduction-electron spin density at the origin and S_z is associated with the impurity. This is just the Kondo Hamiltonian with the transverse parts of the interaction removed. The exact conduction-electron energies corresponding to this model can be obtained by standard potential scattering methods. In particular it is straightforward to use phase shift methods to obtain the following for the scattering states with energies near to the Fermi surface:

$$\varepsilon_{k\sigma}=\varepsilon^0_{k\sigma}-\sigma(1/\pi\rho N)\arctan(\pi\rho J/4)\ . \tag{1.4}$$

The point to be made is that the spin-dependent phase shift, or the effective scattering matrix element at the Fermi surface, and therefore the impurity polarization, is not directly proportional to the exchange interaction except in the small exchange, or weak-coupling, limit. It is this quantity which is chosen implicitly as the invariant charge by Abrikosov and Migdal. In contrast, the contribution the interaction makes to the energy required to make a spin-flip transition of the impurity is simply

$$\Sigma=\tfrac{1}{2}(\rho J)(g\mu_B H)\ , \tag{1.5}$$

and is only linearly dependent upon J even in the strong-coupling, i.e., large-J, limit. This result follows from the examination of longitudinal diagrams, both self-energies and vertex corrections. With (i) particle-hole symmetry and (ii) the usual form of band cutoff, it can be shown that the sum of a given diagram and its particle-hole conjugate obtained by reversing the direction of the conduction-electron lines has no linear term in H, i.e., it is at most $O(H^2)$. Turning to the full Kondo problem, the renormalized exchange is evidently directly related to the derivative $d\Sigma/dH$ but *not* to the effective exchange scattering strength of conduction electrons which involves the arctan of the exchange. In the present approach the invariant charge g is essentially $d\Sigma/dH$, and one is led to study self-consistent equations for Σ.

This philosophy of studying Σ is supported by the observation that the conduction electrons do not have a self-energy in the Dysonian sense. It is necessary to turn to the impurity propagators in order to look for a self-consistent equation for the problem. However, as will be shown, the self-energy of the single d electrons in the

Abrikosov method[11] is not unique. In contrast, the two-particle self-energy Σ is unique.

For counting purposes, the skeleton diagrams in the present approach are mapped onto those associated with Eq. (1.3). The quantity Σ is evaluated by determining the pole of the transverse dynamic susceptibility. It is shown that the longitudinal diagrams generated by the above Hamiltonian can be used as a skeleton set for the evaluation of the diagrams for the full Kondo Hamiltonian. Renormalized diagrams are obtained by first inserting two transverse vertices (denoted TT) for any longitudinal vertex. Then the diagrams can be further renormalized by including the sequence TLT, $TLLT$, etc. The sum $L+TT+TLT+TLLT+\cdots$ corresponds to the usual leading logarithmic or parquet series. The last step [and which would not occur for model (1.3)] is to dress the skeletons, with their renormalized vertices, by including the impurity self-energy. The result will be called the self-consistent parquet approximation.

It seems to be widely appreciated that this type of procedure is complicated by the existence of vertex corrections of the kind illustrated in Fig. 1(a). These $LTLT$ vertex corrections cancel exactly in the evaluation of Σ. This can be shown in one of two ways. First, using the diagram methods developed here these corrections can be arranged in canceling pairs. The second method is to use a variant of the usual Abrikosov method[11] in which such diagrams simply do not exist. However, there still remains a $TTTT$, i.e., $O(J^4)$ purely transverse, vertex correction to the transverse susceptibility, and the methods used to evaluate Σ and put it on its energy shell generate some new types of "overlapping" diagrams which are fully equivalent to regular vertex corrections. These corrections do not cancel quite so handily. However, as will be shown in an appendix they do cancel, in calculation of Σ, in next to leading logarithmic order for an isotropic exchange. Thus the self-consistent parquet approximation is accurate to next to leading order and, in view of the existence of the infrared cutoff discussed above, this will lead to exact results in the scaling limit.

The self-consistent parquet approximation results in an expression of the form:

$$\frac{d\Sigma}{dh}=\tfrac{1}{2}[1/\rho J-(I^{+}+I^{-})]^{-1}-\rho J/2 \tag{1.6}$$

for the derivative of the two-particle self-energy Σ. The quantities $I^{\pm}=\int_0^{\pm D}(\varepsilon+\Sigma-h)^{-1}$ are logarithmic integrals and $h=(1+\rho J/2)g\mu_B H$.

A second differentiation of Eq. (1.6) yields the key result of the self-consistent parquet approximation. It is a universal equation, i.e., one which contains neither the coupling constant nor the band, ultraviolet cutoff:

$$(\Sigma-h)(d^2\Sigma/dh^2)+2(d\Sigma/dh)^2=0\ , \tag{1.7}$$

where again Σ is the self-energy and h the Zeeman energy [the definition of both is modified to $O(J)$, see Sec. V]. While it might not appear so, this will be shown to be equivalent to the scaling equations (1.2a).

The weak-coupling perturbation-theory results determine one of the two integration constants required to integrate Eq. (1.7). This turns out to be the energy scale K for the problem

$$K=-2e^{1/2}D\,|\,\rho J/2\,|^{1/2}\exp(1/\rho J)\ . \tag{1.8}$$

It includes the famous $|\,\rho J\,|^{1/2}$ factor which demonstrates that the next to leading order is correctly accounted for. This integration constant carries the information about the cutoff and coupling constant.

The other integration constant *cannot* be determined by the weak-coupling limit, even in principle. It is determined by requiring that the solution in the strong-coupling limit be explicitly invariant to time reversal. The result is the following expression:

$$4\pi T_0=(e\pi)^{1/2}D\,|\,\rho J\,|^{1/2}\exp(1/\rho J)\ , \tag{1.9}$$

for the energy associated with the pole of the transverse susceptibility and $h=0$. In turn this corresponds to the exact separation between the very much renormalized $S_z=-\frac{1}{2}$ and $\frac{1}{2}$ states of the impurity.

A quantity to be defined as the kink "self-energy" for the single-particle $S_z=\pm\frac{1}{2}$ d-electron propagators also corresponds to exact energies. The expression for these quantities cannot be connected to perturbation theory. However, the strong-coupling limit can be uniquely connected to the above result obtained from the two-particle self-energy. One of the integration constants used to make this connection is obtained by matching the difference in energy between the $S_z=-\frac{1}{2}$ and $\frac{1}{2}$ energies to $4\pi T_0$. The second is again obtained by time-reversal symmetry.

With a knowledge of the effective coupling constant the quasiparticle energies can be calculated. From these is obtained the density of states, the susceptibility, and the specific heat. The result is

$$\chi=(\mu_B)^2/\pi T_0 \tag{1.10}$$

in agreement with the result of Wilson.[1,3] The specific heat corresponds to a Wilson ratio $R=2$, and the energy correction at the Fermi surface corresponds to a phase shift $\delta=\pi/2$.

With use of these results for the quasiparticle energies, it is then possible to construct the conduction-electron t matrix and confirm that it reaches the unitarity value $1/i\pi$. This also gives an expression for the resistivity relaxation time.

To calculate conduction-electron properties, in general, a part of the longitudinal series must be accounted for. Because of this the conduction electron and other physical quantities involve, again in general, an expansion in the present effective interaction vertex defined as g. For the weak-coupling limit this will yield the usual asymptotic expansion. However, in the strong-coupling limit the result is simpler. The shift in the energies of the quasiparticles is proportional to g. Exact results are recovered for the specific heat and susceptibility via a calculation of the density of states for the quasiparticles. Again all relevant vertex corrections to the conduction-electron self-energies such as those of the structure shown in Fig. 1(d) are included, as needed.

In addition to the nonstandard Abrikosov representation and the techniques used to define two-particle self-

energies, other unusual diagram methods are used. It is desired that the quasiparticle energies be obtained directly from the evaluation of the conduction-electron propagator. As discussed at length for example in the recent book of Mahan,[12] even for plain potential scattering it is usually *not* the case that the real part of the conduction-electron self-energy (defined for many impurities after Kohn and Luttinger[13]) corresponds to the quasiparticle energies. The standard method would be to calculate the phase shift δ from the t matrix and use the result that the energy shift is $\delta/\pi\rho N$, for a single impurity. Here it is shown by way of example, for this same simple potential scattering problem, that the quasiparticle energies can be recovered directly, provided care is taken in treating the infrared cutoff. For the potential scattering problem the relevant infrared cutoff is $2D/N$, $2D$ being the bandwidth and N the number of electrons per band. This is the separation between adjacent conduction-electron states. Even for the single-impurity problem it is possible to define a quantity which plays the role of a "self-energy," but which will always be referred to in quotation marks to distinguish it from the self-energy defined by Dyson's equation. As noted above the latter does not exist for a single impurity. In contrast to the potential scattering problem, the Kondo problem is shown to have an intrinsic infrared cutoff associated with the energy required to excite the impurity and which is of the order of the Kondo temperature $4\pi T_0$. This greatly exceeds the conduction-electron cutoff $2D/N$ and permits the single-impurity "self-energy" to be more easily defined. This method is used to obtain the quasiparticle energies. The results are then combined with the conventional definition of the t matrix to obtain a useful formula for the conduction-electron propagator and from this the resistivity.

A second novel quantity is denoted as the kink "self-energy." A technique of repeated partial fraction expansions is used to define these quantities which are used in the systematic evaluation of an appropriate energy shell for various Dysonian d-electron self-energies. This technique is particularly useful in the evaluation of the d-electron occupation numbers. In essence the technique converts the Feynman expansion into a Rayleigh-Schrödinger perturbation series.

The Hamiltonian and the two versions of the Abrikosov representation used in this work are introduced in Sec. II. A discussion of the relevance of the infrared cutoff for the problem of potential scattering is given in Sec. III. Also in this section is found the rational behind the definition of kink "self-energies," and described is the evaluation of an $O(J^2)$ vertex correction to an $O(J^2)$ self-energy. In Sec. IV the method of defining two-particle self-energies is reviewed and illustrated. Section V describes the construction of the self-consistent parquet approximation for the two-particle self-energy. The relation of the results of Sec. V to conventional scaling is discussed in Sec. VI. The solution of the universal equation (1.7) is matched to the relevant weak-coupling expansion in Sec. VII. The precise definition of the integration constant K and its relation to the high-field scale T_H is detailed. The strong-coupling limit is the subject of Sec. VIII. The value of the effective coupling constant g in this limit is determined, this being equivalent to determining the second integration constant for Eq. (1.7). The occupation numbers for the d electrons are calculated in Sec. IX. This involves some further development of the kink methods introduced in Sec. III. The impurity polarization is calculated from these results and the total compensation of the impurity moment is discussed. The quasiparticle energies are calculated in Sec. X. From these the susceptibility and specific heat are obtained. These determine the Wilson ratio R. With use of the results for the quasienergies, the usual t matrix can be uniquely determined and the resistivity time calculated. Finally, Sec. XI contains a summary and conclusions along with a short discussion of the applicability of the present methods to the single-impurity Anderson model[14] and the lattice problems. An appendix contains some of the details pertaining to the cancellation of the omitted $O(J^4)$ vertex corrections and dressings.

II. HAMILTONIAN AND FORMULATION

The Hamiltonian studied in this work is essentially the standard s-d exchange or Kondo Hamiltonian:

$$H=\sum_{k,\sigma}\varepsilon_{k\sigma}n_{k\sigma}-(J/N)\sum_{k,k'\sigma\sigma'}a^{\dagger}_{k\sigma}(\mathbf{S}\cdot\mathbf{s}+\tfrac{1}{4})_{\sigma\sigma'}a_{k'\sigma'}\,. \quad (2.1)$$

Here $\mathbf{S}$ refers to the spin of the impurity and $\mathbf{s}$ to that of the conduction electrons. The index σ denotes the conduction-electron spin index. $a_{k\sigma}$ and $n_{k\sigma}$ are the destruction and number operators. A given impurity spin operator $\tilde{O}$ is replaced by a pseudofermion operator according to[11]

$$\tilde{O}\rightarrow\sum_{s,s'}d^{\dagger}_{s}\langle s\,|\,\tilde{O}\,|\,s'\rangle d_{s'}\,. \quad (2.2)$$

Here the impurity spin ket $|\,s\rangle=|\,\pm\tfrac{1}{2}\rangle$ as $s=\pm1$ or $\uparrow$ and $\downarrow$. The unphysical pseudofermion states are projected out by adding a term

$$H_{\lambda}=\lambda(d^{\dagger}_{\uparrow}d_{\uparrow}+d^{\dagger}_{\downarrow}d_{\downarrow}) \quad (2.3)$$

and taking the limit $\lambda\rightarrow\infty$. The pseudovacuum with no "d" electrons never contributes to the expectation value of any term in Wick's theorem since in the interaction a d-destruction operator always lies to the right. The states with a single up or down d electron correspond to the equivalent impurity spin state. Expectation values involving these states contain a Boltzmann factor $f=\exp(-\beta\lambda)$, $\beta=1/k_BT$. States with more d fermions are higher in energy by multiples of λ; the corresponding Boltzmann factors are powers of f and these states do not contribute. In well-known fashion, this results in there being no linked cluster theorem and the usual result that the partition function cancels against the vacuum polarization diagrams when evaluating that a Green's function is no longer valid. It is necessary to explicitly calculate the partition function, at least in principle. In addition to the usual prescription for this quantity there is a special, simple rule associated with the Abrikosov projection technique (see Sec. IX).

It turns out that diagrams with n loops involve f^n, i.e., only one impurity loop occurs in any given diagram. This will be referred to as "the single-loop rule."

When applied to the Hamiltonian H, from Eq. (2.1), the replacement formula, Eq. (2.2), is not unique. For exam-

ple, (2.1) can be written in terms of d electrons, by setting either $\tilde{O}=\mathbf{S}\cdot\mathbf{s}$ or $\tilde{O}=P=(\mathbf{S}\cdot\mathbf{s}+\frac{1}{4})$. The result, and corresponding diagram rules, are different. More specifically the latter approach leads to an interaction of the form

$$-(J/N)\sum_{\sigma,\sigma';k,k';s,s'} a^{\dagger}_{k\sigma}d^{\dagger}_{s}(\mathbf{S}\cdot\mathbf{s}+\tfrac{1}{4})_{\sigma\sigma',ss'}a_{k'\sigma'}d_{s'}\,, \quad (2.4)$$

which involves the physically nonsensical replacement $\frac{1}{4}\rightarrow\frac{1}{4}(d^{\dagger}_{\uparrow}d_{\uparrow}+d^{\dagger}_{\downarrow}d_{\downarrow})$. The former replacement corresponds to an interaction:

$$-(J/N)\left[\sum_{\sigma,\sigma';k,k';s,s'} a^{\dagger}_{k\sigma}d^{\dagger}_{s}(\mathbf{S}\cdot\mathbf{s})_{\sigma\sigma',ss'}a_{k'\sigma'}d_{s'} + \sum_{\sigma,k,k'}\tfrac{1}{4}a^{\dagger}_{k\sigma}a_{k'\sigma}\right] \quad (2.5)$$

with which the potential scattering term does not involve d operators. From the point of view of diagram structure, and for impurity quantities, the former method is simpler and will be used for that purpose. Conduction-electron quantities will be calculated with the standard method. Clearly physical results cannot depend upon which of the methods is used. The calculation can be done with either method; however, some summations are easier to do with one method rather than the other.

The d-electron propagators are represented by the wavy lines shown in Fig. 2, while the conduction electrons correspond to straight lines. The various vertices are also illustrated in Fig. 2. The spin-flip or transverse vertices are standard; however, with the interaction in the form of Eq. (2.4), there is only the one longitudinal vertex involving uniquely lines with the same value of the spin. The matrix element for each such vertex, both longitudinal and transverse, has a value of 1/2.

An important point which never seems to have surfaced in the literature on this method is the fact that the d-electron self-energy is not unique. The above two ways of representing the potential scattering term properly illustrate the problem and its origin. Consider the $O(J^2)$ self-energies shown in Fig. 3. In the absence of a field the integrals involved in both the transverse and longitudinal contributions are the same; however, in the representation of the interaction corresponding to Eq. (2.5) the longitudinal contribution has different matrix elements, and despite the sum on the spin index is one-half the transverse term. In contrast, with Eq. (2.4) the two contributions are equal under the same circumstances. The reason is simple. Involved is the propagator $\langle T_{\tau}d^{\dagger}_{s}(\tau)d_{s}(0)\rangle$. The destruction operator d_s, acting on a physical state, not only destroys the single d electron but also destroys the interaction; this because another destruction d operator always lies to the right in the interaction and cannot act (with a finite result) on the d-electron vacuum. The inverse argument applies for the reversed time ordering. When the potential scattering is written in terms of d operators, this results in the potential being "turned on" or "off" at $\tau=0$, which in well-known fashion leads to an infrared divergence and the extra self-energy contribution. Clearly the d-electron self-energy cannot have any real physical meaning. However, when summed over its external frequency the d-electron propagator gives the occupation numbers. Since these *do* have physical meaning the result must be unique. The calculation of these quantities is described in Sec. IX.

III. DIAGRAM METHODS

A few unusual methods are used in the present diagram development. In one form or another most of these have appeared in the author's previous work.[6,9,15] This section and the beginning of the next review these techniques in the context of the present problem.

One innovation involves the systematic evaluation of two-particle or higher-order propagators using repeated partial fraction expansions. This is to be found in the next section. In this section the same type of systematic expansion is used to develop a "kink" method for studying single-particle propagators. Involved is the question of the appropriate energy argument for a self-energy when it is put on its "energy shell."

A second topic is the role of vertex corrections. While, as stated in the Introduction, there are no skeleton $O(J^2)$ vertex corrections to the important transverse self-energies when the alternative Abrikosov method is used, there are equivalent contributions generated by certain overlapping and the kink self-energies. The evaluation of these is identical to the evaluation of the vertex corrections with the standard Abrikosov method. The evaluation of the $O(J^2)$ vertex corrections to the $O(J^2)$ transverse self-energy will be described at the end of this section. This serves to illustrate the role of such terms both in connection with the particular diagram and in relation to the other types of corrections which arise later in this paper.

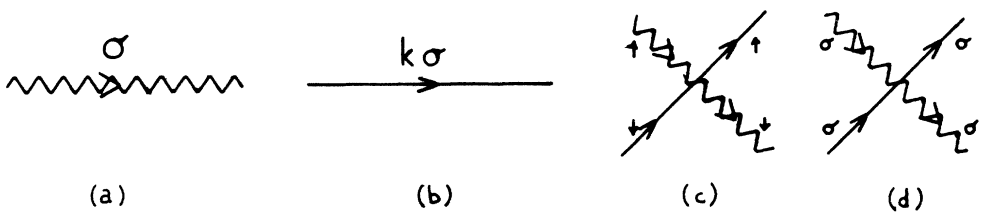

FIG. 2. (a) Wavy lines represent the magnetic impurity propagator. The Abrikosov representation of the impurity sign operators is used, see Sec. II. (b) Straight lines correspond to conduction-electron propagators. (c) illustrates the transverse vertex while (d) shows that in a nonstandard Abrikosov representation the only longitudinal vertex involves propagators with the same spin. Both this and the more standard representations will be used. In the standard version of the Abrikosov representation the spin of the impurity and conduction-electron propagator may differ.

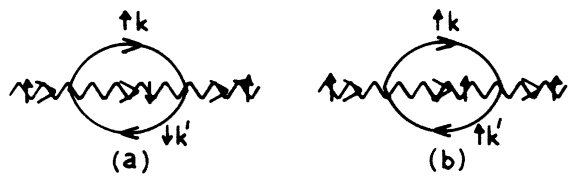

FIG. 3. (a) Transverse d-electron self-energy. The matrix elements contribute a factor $(\frac{1}{2})^2$. (b) The longitudinal contribution depends upon the type of Abrikosov representation used. In the standard representation there is a spin sum to give a prefactor 2 times $(\frac{1}{4})^2=\frac{1}{8}$, while for the same contribution in the nonstandard method there is no spin sum but the matrix elements are twice the size to give a factor $(\frac{1}{2})^2=\frac{1}{4}$, twice the size.

First, however, as an aside, the problem of plain potential scattering will be considered. The purpose is to focus upon the different ways of treating the energy shift of the quasiparticles. This problem is discussed at some length in the recent book by Mahan;[12] it is assumed that the reader is familiar with the standard methods at this level.

Consider the simplest Hamiltonian possible:

$$H=\sum_k \varepsilon_k^0 n_k+(v/N)\sum_{k,k'} c_k^\dagger c_{k'} , \tag{3.1}$$

where it is assumed that there is a constant density of states ρ lying between ultraviolet cutoffs at $\pm D$, v is the potential scattering strength and there is assumed to be one electron per band. For a finite system of N states per band there will also be an infrared cutoff $2D/N$ corresponding to the separation between individual levels.

Rather than using the Kohn and Luttinger[13] method of averaging over many impurities, here the single scattering center problem will be considered. Repeated scattering from the center can still be represented by diagrams of the form shown in Fig. 4. However, such a diagram is proportional $(1/N)$ rather than the concentration c, and there is no self-energy in the Dysonian sense. So much is standard and leads to the following for the conduction-electron Green's function:

$$G_k(\varepsilon+is)=(\varepsilon+is-\varepsilon_k^0)^{-1}\left[1+(v/N)\left[1-(v/N)\sum_{k'}(\varepsilon+is-\varepsilon_{k'}^0)^{-1}\right]^{-1}(\varepsilon+is-\varepsilon_k^0)^{-1}\right] . \tag{3.2}$$

If the sum is converted into an integral,

$$(1/N)\sum_{k'}(\varepsilon_{k'}^0-\varepsilon+is)^{-1}=\rho\int_{-D}^{D} d\varepsilon'(\varepsilon'-\varepsilon-is)^{-1}=\rho\{i\pi+\ln[(D-\varepsilon)/(D+\varepsilon)]\} , \tag{3.3}$$

provided of course the energy ε lies within the band.

This Green's function equation defines a t matrix:

$$\begin{aligned} t_{k,k}&=(v/N)/[1+(\rho v)i\pi] \\ &=e^{i\delta}(v/N)/[1+(\rho v)^2\pi^2]^{-1/2} , \end{aligned} \tag{3.4}$$

where the logarithmic term in Eq. (3.3), which is negligible for energies close to the Fermi surface, has been omitted. The phase shift δ is given by

$$\delta=\tan^{-1}(\rho\pi v) . \tag{3.5}$$

This phase shift corresponds to an energy correction $\Delta\varepsilon=\delta/\rho\pi N$. When $v\to\infty$ this gives the unitarity limit $\delta=\pi/2$, $t=1/Ni\pi\rho$, or $\Delta\varepsilon=D/N$. All of this is again standard.

It should be, and is, possible to obtain the phase shift formula

$$\Delta\varepsilon=\delta/\pi N=(1/\pi\rho N)\tan^{-1}(\rho v\pi)$$

without introducing the imaginary parts of the self-energy, simply by taking the continuum limit in a different way. If it is assumed that the infinitesimal $s<2D/N$, the infrared cutoff, then the imaginary parts of the self-energies will be suppressed. However, it is not correct that when this is done the real part of the "self-energy" is given by the logarithmic term above; one must be careful to account for the discrete nature of the sum in Eq. (3.3). The more or less standard way to do this is to find the exact poles of the t matrix, i.e., to solve for the roots of

$$1/v-(1/N)\sum_{k'}(\varepsilon_{k'}-\varepsilon+is)^{-1}=0 . \tag{3.6}$$

This is not difficult to do analytically, although the author has never seen the details reproduced in the literature. It is necessary to explicitly perform the sum taking account of the infrared cutoff. The sum is of the form

$$S=\sum_{n=-N/2}^{N/2}[(n'-n)+\tfrac{1}{2}+x]^{-1} , \tag{3.7}$$

where it is intended that the correction $x=\rho\Delta\varepsilon_n$ from the unitary, or large v limit, is to be evaluated, i.e.,

$$\varepsilon_k=(2D/N)(n+\tfrac{1}{2})+\Delta\varepsilon_n/N ,$$

where the unperturbed energy is $\varepsilon_k^0=(D/\pi)k$, $k=(2\pi/N)n$ with n lying in the interval $-N/2$ to $N/2$. The sums can be evaluated in terms of ψ functions $\psi(x)$:

$$\sum_{n=0}^{N-1}(n+x)^{-1}=\psi(N+x)-\psi(x) . \tag{3.8}$$

The result is

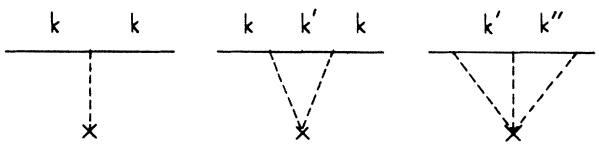

FIG. 4. Diagrams which represent the repeated scattering of conduction electron from a static potential.

$$S=\ln\{[N/2+\tfrac{3}{2}-(n-x)]/[N/2+\tfrac{3}{2}+(n-x)]\}$$
$$-\pi\tan(\pi x)\,, \tag{3.9}$$

where the large N result $\psi(N)\sim\ln N$ and the identity

$$\psi(\tfrac{1}{2}+x)-\psi(\tfrac{1}{2}-x)=\pi\tan(\pi x)$$

have been used. The logarithmic term in the sum S is simply $\ln[(D-\varepsilon)/(D+\varepsilon)]$. If, consistent with Eq. (3.4), this is ignored the expected equation for the roots is

$$1/v-\rho\pi\tan(\pi\rho\,\Delta\varepsilon_n)=0\,, \tag{3.10}$$

or

$$\Delta\varepsilon_n=(1/\rho\pi)\tan^{-1}(1/\rho\pi v) \tag{3.11}$$

which agrees with Eq. (3.5).

The same arithmetic can be used to obtain an effective "self-energy" σ directly. Now care must be taken to treat separately the terms in the sum for which $k'=k$; in particular,

$$\sum_{k'}(\varepsilon^0_{k'}-\varepsilon+is)^{-1}=\sum_{k'(\neq k)}(\varepsilon^0_{k'}-\varepsilon+is)^{-1}+(\varepsilon^0_k-\varepsilon+is)^{-1}$$
$$=\rho NS'+(\varepsilon^0_k-\varepsilon+is)^{-1} \tag{3.12}$$

is the correct way to separate the sum when evaluating G_k. Inserting the result into the expression for G_k gives

$$G_k(\varepsilon+is)=(\varepsilon+is-\varepsilon^0_k)^{-1}\{1+(v/N)[1-(v/N)S-(v/N)(\varepsilon+is-\varepsilon^0_k)^{-1}1^{-1}(\varepsilon+is-\varepsilon^0_k)^{-1}\}$$
$$=\{\varepsilon+is-[\varepsilon^0_k+\sigma(\varepsilon)]\}^{-1}\,. \tag{3.13}$$

On its energy shell the "self-energy" is given by

$$\sigma=(v/N)[1-(v/N)S']^{-1}\,, \tag{3.14}$$

where

$$S'=S(\varepsilon=\varepsilon_k)-(\tfrac{1}{2}+x)^{-1} \tag{3.15}$$

is again the sum with the $k=k'$ term excluded. Δs before the effects of the ultraviolet cutoff, i.e., band-edge effects, are ignored by dropping the logarithmic term. Substituting for α and using the definition of x then gives

$$\sigma=(1/\rho N)(\tfrac{1}{2}+\rho\,\Delta\varepsilon_n)$$
$$=(1/N\rho)[\tfrac{1}{2}+(1/\pi)\tan^{-1}(1/\rho\pi v)]\,, \tag{3.16}$$

which again is the exact answer, with band-edge effects ignored. On the energy shell $\sigma(\varepsilon=\varepsilon_k)$ is smooth. In contrast, as a function of ε it is highly singular with singularities separated by $2D/N$, the infrared cutoff.

There are two conclusions to be drawn from this simple example. First, if the continuum limit is taken correctly, it is possible to suppress the imaginary parts of the self-energies and obtain directly the results usually calculated via a phase shift analysis. Second, the infrared cutoff is the energy scale upon which such a real $\sigma(\varepsilon)$ is singular.

In connection with the present problem it is desirable to exploit these observations. Because scattering involves excitation of the impurity, for the Kondo problem it will be found that the infrared cutoff is of the order of the Kondo energy $4\pi T_0$, and therefore, unlike for this example, does *not* go to zero in the thermodynamic limit, $N\to\infty$.

The second subject to be covered in this section is the systematic evaluation of the appropriate "energy shell" using repeated partial fraction expansions. These will be called kink methods.

The basic partial fraction expansion is, e.g.,

$$[\varepsilon_k-i(\omega_n+\omega_0)]^{-1}[\varepsilon_{k'}-i\omega_n]^{-1}=(\varepsilon_k-\varepsilon_{k'}-i\omega_0)^{-1}\{[\varepsilon_{k'}-i\omega_n]^{-1}-[\varepsilon_k-i(\omega_n+\omega_0)]^{-1}\}\,.$$

This identity is correct and is used repeatedly in this paper. No difficulty arises when the results are continued to the real axis ($i\omega_0\to\varepsilon+is$) *except* in connection with the presently discussed kink methods when both the complex frequencies, ω_n and $\omega_n+\omega_0$, are the same. Then, on the real axis, one must use the identity

$$[\varepsilon_k-(\varepsilon+is)]^{-1}[\varepsilon_{k'}-(\varepsilon+is)]^{-1}$$
$$=[(\varepsilon_k-\varepsilon)^{-1}+i\pi\delta(\varepsilon_k-\varepsilon)][(\varepsilon_{k'}-\varepsilon)^{-1}+i\pi(\varepsilon_{k'}-\varepsilon)]$$
$$=(\varepsilon_k-\varepsilon)^{-1}(\varepsilon_{k'}-\varepsilon)^{-1}+[(\varepsilon_{k'}-\varepsilon)^{-1}i\pi\delta(\varepsilon_k-\varepsilon)+(\varepsilon_k-\varepsilon)^{-1}i\pi(\varepsilon_{k'}-\varepsilon)]-\pi^2\delta(\varepsilon_k-\varepsilon)\delta(\varepsilon_{k'}-\varepsilon)$$
$$=(\varepsilon_{k'}-\varepsilon_k)^{-1}[(\varepsilon_k-\varepsilon)^{-1}+i\pi\delta(\varepsilon_k-\varepsilon)-(\varepsilon_{k'}-\varepsilon)^{-1}-i\pi(\varepsilon_{k'}-\varepsilon)]-\pi^2\delta(\varepsilon_k-\varepsilon)\delta(\varepsilon_{k'}-\varepsilon)$$
$$=(\varepsilon_{k'}-\varepsilon_k)^{-1}\{[\varepsilon_k-(\varepsilon+is)]^{-1}-[\varepsilon_{k'}-(\varepsilon+is)]^{-1}\}-\pi^2\delta(\varepsilon_k-\varepsilon)\delta(\varepsilon_{k'}-\varepsilon)\,. \tag{3.17}$$

When a denominator does not contain "is" a principle part is implied.

However, it must be realized that the $\pi^2\delta(\varepsilon_k-\varepsilon)\delta(\varepsilon_{k'}-\varepsilon)$ term is only present when both the variables ε_k and $\varepsilon_{k'}$ have a continuous spectrum. This is the case, for this example, when the thermodynamic limit is taken in the usual way, i.e., when $s>D/N$, D being the bandwidth. In Sec. IX, where extensive use is made of these kink methods, the thermodynamic limit is in fact taken in the unconventional way with $s<D/N$ and these terms do not arise.

In Sec. V, which uses the conventional thermodynamic limit, is is added to the first denominator in the last line of (3.17). This does not alter anything:

$$[\varepsilon_k-(\varepsilon+is)]^{-1}[\varepsilon_{k'}-(\varepsilon+is)]^{-1}=(\varepsilon_{k'}-\varepsilon_k-is)^{-1}\{[\varepsilon_k-(\varepsilon+is)]^{-1}-[\varepsilon_{k'}-(\varepsilon+is)]^{-1}\}-\pi^2\delta(\varepsilon_k-\varepsilon)\delta(\varepsilon_{k'}-\varepsilon)\,, \tag{3.18}$$

since the coefficient of the extra δ function is zero. The choice (3.18) will result in the self-energies having their expected imaginary parts. When this is done the term $\pi^2\delta(\varepsilon_k-\varepsilon)\delta(\varepsilon_{k'}-\varepsilon)$ is not involved in the definition of the kink self-energy discussed here and in Sec. V. When the remainder is required these extra terms arising from the product of two or more δ functions must be accounted for separately. This will not occur in the present work.

The aim of the kink procedure as outlined in this section is to give a regular self-energy an argument appropriate to the "energy shell" of the relevant propagator. The technique will be illustrated with a single d-electron propagator, although an important application of the method, found in Sec. V, is in relation to the impurity dynamic susceptibility, a two-particle propagator within the present method. The energy shell is defined as being the energy ε_s, the solution of an equation of the form

$$\varepsilon_s-[\Sigma(\varepsilon_s)+\lambda+\sigma h/2]=0\ . \tag{3.19}$$

In general, the determination of ε_s involves the continuation of Σ beyond the cut on the real axis. Clearly, putting a self-energy on its energy shell effectively includes the self-energy in the argument of the self-energy itself as a part of the exact energy ε_s; this rather than, say, giving the self-energy the argument $\lambda+\sigma h/2$, i.e., the unperturbed value for the energy shell for the d propagator. The kink methods develop a systematic expansion for the quantity $\Sigma(\varepsilon_s)$. If taken to infinite order these methods would give this quantity exactly. The point of the exercise is to develop a method which can be used to justify an approximate expression for the same quantity.

Consider the d-electron propagator evaluated with just the bare $O(J^2)$ transverse self-energy as implied by the Dyson equation illustrated in Fig. 5. This self-energy corresponds to an expression of the form

$$(J/N)^2\sum_{k,k'}n_{k'}(1-n_k)/[i\omega_n-(\lambda-h/2+\varepsilon_k-\varepsilon_{k'})]\ . \tag{3.20}$$

Notice that the projection energy λ appears in the denominator and with this level of approximation the expression corresponds to the sum of simple poles. The first step is to make a partial fraction expansion between the self-energy denominator and an undressed d-electron propagator, the two parts on the right-hand side connected by the arrow labeled 1. The result is illustrated by the kinked diagrams shown in the first line of Fig. 6. The denominator which is the result of the expansion and which no longer contains the external frequency ω_n corresponds to taking a cut though the *vertical* part of the diagram. For each propagator with a *horizontal* part there is a corresponding denominator which contains ω_n. Each partial fraction expansion removes one horizontal section of the diagram but, at least, doubles the number of these new types of diagrams.

In this section only the kinked diagrams, such as those to the extreme right of the top line in Fig. 6 which contribute to the kink "self-energy," will be considered. Explicitly the kink "self-energy" has a value

$$(J/N)^2\sum_{k,k'}n_{k'}(1-n_k)/(\varepsilon_k-\varepsilon_{k'}-h)\ . \tag{3.21}$$

This corresponds to the bare self-energy with a bare energy shell. Since only the d line can be dressed, because of the single-loop rule, the exact regular self-energy is of the form

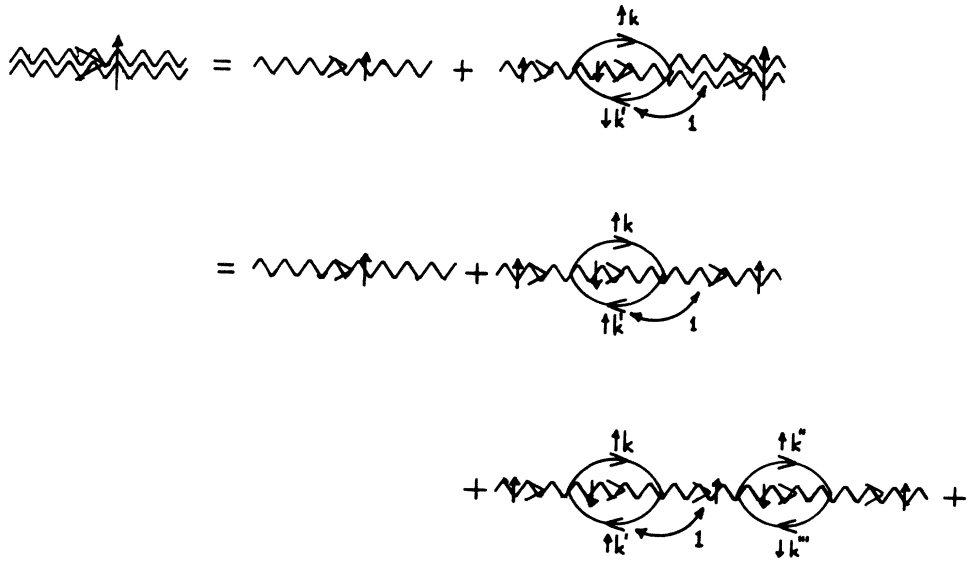

FIG. 5. Dyson's equation in which only a single $O(J^2)$ transverse self-energy has been included. The initial partial fraction expansion used in the kink method is between the denominator of the self-energy and the first bare propagator in the development of the full propagator. Compare the two lines on the right-hand side. In the second line the quantities connected by the arrow marked 1 are the ones expanded. The same arrow in the first line is intended as a shorthand notation.

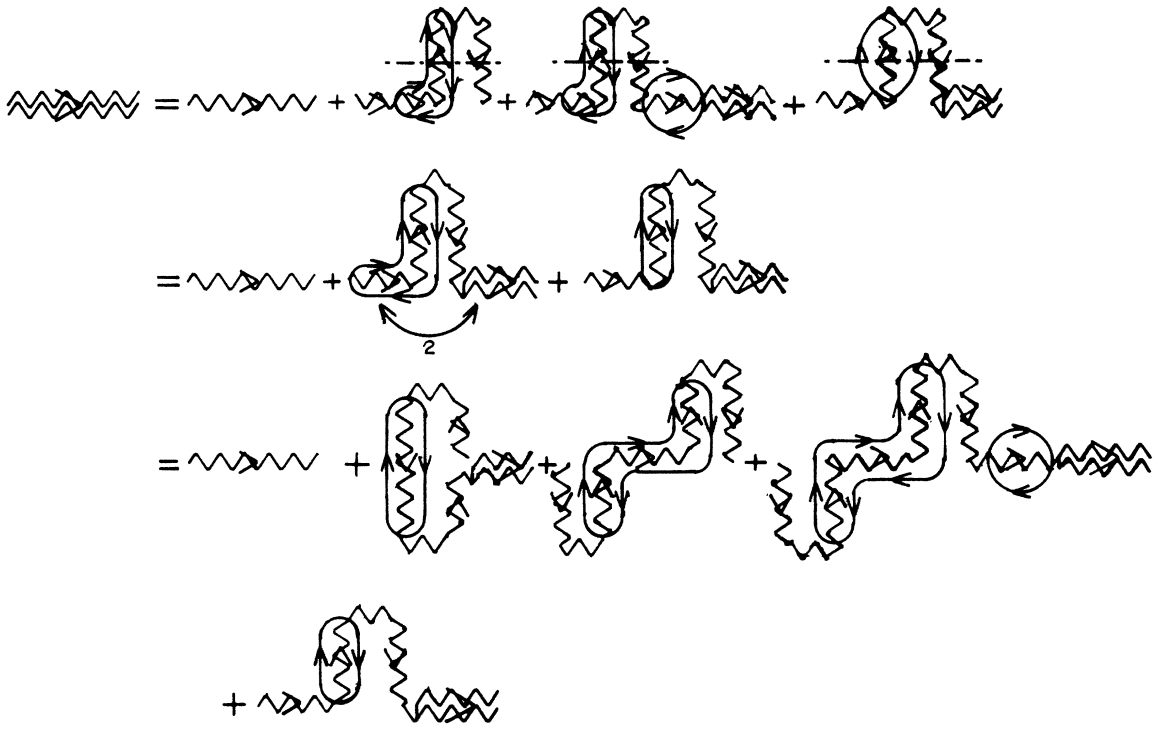

FIG. 6. Top line shows the result, in diagrams terms, of the partial fraction expansion indicated by arrow 1 in Fig. 5. The denominator, the result of the expansion, does not contain the external frequency. The corresponding energy denominator is obtained by making a horizontal cut through the vertical, or kinked, part of the diagram. Each such expansion, in essence, doubles the number of contributions, although, as here more than double the number of diagrams are required to represent the various contributions. See the text.

$$(J/N)^2 \sum_{k,k'} n_{k'}(1-n_k)/\{i\omega_n - [\Sigma_\downarrow(\varepsilon_{k'}-\varepsilon_k+i\omega_n)+\lambda-h/2+\varepsilon_k-\varepsilon_{k'}]\} , \tag{3.22}$$

where $\Sigma_\downarrow$ is the exact, regular self-energy. Repeated partial fraction expansions generate terms which form a series to give the result illustrated in Fig. 7 and which includes the up-spin self-energy $\Sigma_\uparrow$, with a specific argument, in the denominator of the original up-spin self-energy to give a dressed kink self-energy:

$$(J/N)^2 \sum_{k,k'} n_k(1-n_{k'})/[\Sigma_\downarrow(\varepsilon_k-\varepsilon_{k'}+h/2)-\Sigma_\uparrow(\varepsilon_{k'}-\varepsilon_k-h/2)-h+\varepsilon_k-\varepsilon_{k'}] . \tag{3.23}$$

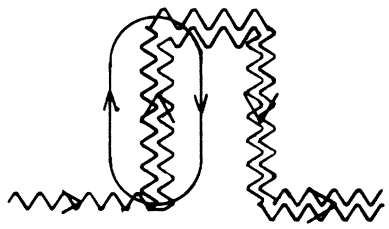

FIG. 7. Illustrated is the dressed kink self-energy. Not only is the d propagator in the interior of the original single-particle self-energy dressed, in addition the antiparallel external line which determines the argument of the self-energy is also dressed. This latter dressing introduces a second self-energy in the denominator of the self-energy itself. The kink method thereby specifies an energy shell for the single-particle self-energies, this including self-energy corrections to that energy shell. The small horizontal portion at the top of the diagram is included for clarity and does not correspond to a propagator. Here, and in other diagrams, such parts will not have an arrow attached.

With this partial fraction expansion technique the self-energy again appears in the argument of the self-energy, but now it involves the intermediate-state energy in a manner which is equivalent to the way the self-energy, which is the dressing of the internal down d line, contains the same energy. This form is more useful for the present development. The relation to the more standard prescription Eq. (3.19) is discussed below and in connection with the construction of the parquet approximation in Sec. V. Other terms generated by this kink method are involved. These are "overlapping" kink self-energies such as that illustrated in Fig. 8 and come from higher-order terms in the partial fraction expansion. Such terms are fully equivalent to vertex corrections of the same order, and in particular this diagram must, in principle, be accounted for since it is of next to leading order. The fact that there is a cancellation of such terms to that degree of approximation is important.

In Sec. V this technique will be used to deduce the appropriate energy shell for what will be defined as a two-

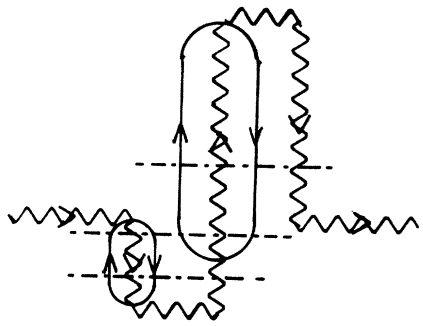

FIG. 8. Double kinked self-energy. The three denominators without an external frequency correspond to the three horizontal lines. These overlapping contributions are equivalent to vertex corrections. These will discussed in connection with other overlapping two-particle self-energies to be defined later and actual vertex corrections.

particle self-energy. In Sec. IX the terms omitted in the above will be evaluated in order to obtain the d-electron occupation numbers. It will be seen that the omitted terms involve the derivatives of the same kink self-energies.

The last topic in this section is the evaluation of vertex corrections. Consider the $O(J^4)$ diagram shown in Fig. 9(a). This can be viewed as a transverse vertex correction to the $O(J^2)$ transverse self-energy. When placed upon the energy shell (i.e., to this level of approximation, with the external frequency $\omega_0=h$, the Zeeman energy) the contribution turns out to be of the form

$$N\frac{1}{h-(\varepsilon_{k''}-\varepsilon_{k'''})}\frac{1}{h-[(\varepsilon_k-\varepsilon_{k'})+(\varepsilon_{k''}-\varepsilon_{k'''})-h]}\times\frac{1}{h-(\varepsilon_k-\varepsilon_{k'})}, \quad (3.24)$$

where $N=J^4(1-n_k)n_{k'}(1-n_{k''})n_{k'''}$ is the numerator. Extraneous factors have been omitted and there is an implicit sum upon the k values. The vertex corrections in the regular Abrikosov method are, to within the magnetic field arguments and sign, of the same general form. (But see below for a specific statement about such corrections.) This contribution should be compared with the first term generated by dressing the internal d propagator. This is shown in Fig. 9(b) and has the value

$$N\frac{1}{h-(\varepsilon_k-\varepsilon_{k'''})}\frac{1}{h-[(\varepsilon_k-\varepsilon_{k'})+(\varepsilon_{k''}-\varepsilon_{k'''})-h]}\times\frac{1}{h-(\varepsilon_k-\varepsilon_{k'})} \quad (3.25)$$

with the same conventions. Making a partial fraction expansion between the first two denominators in the vertex correction gives one term which cancels this dressing and leaves a net result:

$$N\frac{1}{h-(\varepsilon_k-\varepsilon_{k'})}\frac{1}{h-(\varepsilon_{k''}-\varepsilon_{k'''})}\frac{1}{h-(\varepsilon_k-\varepsilon_{k'})}. \quad (3.26)$$

This factors into two sets of independent sums and gives a net contribution of the form:

$$\frac{\partial\Sigma^{(2t)}}{\partial\varepsilon}\Sigma^{(2t)} \quad (3.27)$$

which is just the first term in a Taylor expansion which would give eventually Eq. (3.19).

The role of these overlapping bubble vertex corrections should be clear from a comparison between (3.25), which corresponds to the $O(J^2)$ dressing of the $O(J^2)$ self-energy, and (3.26), which is the sum of the vertex correction and the same dressed self-energy. The central denominator in (3.25) corresponds to the self-energy within the self-energy. Since it involves the energies ε_k

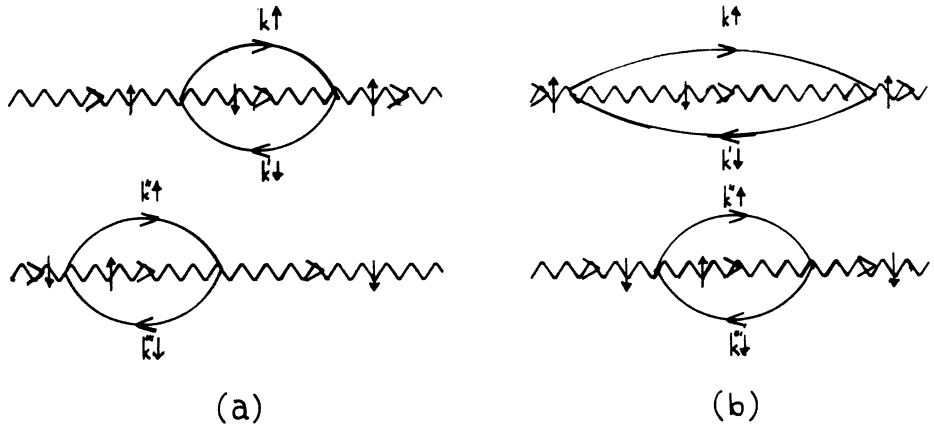

FIG. 9. (a) Overlapping $O(J^4)$ two-particle self-energy. The precise definition of these are given in Sec. IV. They are fully equivalent to the usual $O(J^4)$ vertex correction of the form illustrated in Fig. 1(a). However, with the nonstandard Abrikosov representation used here such vertex corrections do not occur. (b) The overlapping term cancels, in part, against this dressing of the two-particle self-energy. Again the definitions are given in the next section.

and $\varepsilon_{k'}$ it is definitely not on the energy shell of the impurity propagator. However, when the vertex correction is included the result (3.26) is of the same mathematical form except now these energies no longer appear, i.e., the sum of the dressing to the self-energy and the vertex correction is the same as if the dressing alone were put on the internal impurity line energy shell.

This is always the role of these important, i.e., next to leading logarithmic, contributions which arise from $O(J^2)$ vertex corrections and higher-order similar corrections *which are due to diagram overlap.* They replace the dressing of the internal d propagator by it's value on the d-propagator energy shell.

However, for direct vertex corrections, such as those in Fig. 1(a), this is not necessarily so. In particular, in Fig. 1(a) the two longitudinal vertices have different signs, and as a result such a vertex correction would double rather than cancel the similar fourth-order dressing while, in addition, making a contribution similar to, but the negative of, Eq. (3.26). Also, it is reiterated that the cancellation result is only valid for the relevant initial self-energies placed on its energy shell.

This result, however, is useful in Sec. V and the Appendix to show that, for an isotropic exchange (i.e., $J\mathbf{S}\cdot\mathbf{s}$) interaction, the overlapping vertex corrections cancel. Other "regular" vertex corrections will be either shown to cancel against each other or are accounted for with the necessary precision.

IV. TWO-PARTICLE SELF-ENERGIES

It is not usual (see, e.g., Ref. 12) to define a two-particle self-energy, although the method used here appeared in the literature over a decade ago.[9] A two-particle self-energy is defined as a repeated inclusion in a two-particle propagator which modifies the energy of the pole, or poles, of that propagator. The definition presented here is unique if a few minimum requirements are made of a quantity which passes by that name.

Traditional methods for dealing with two-particle propagators tend to treat vertex corrections in quite a different way from single-particle self-energies, although it is known they can sometimes be related via Ward identities. Barnes and Zitkova-Wilcox[9] have shown that, in fact, they can be treated in a very similar fashion. The methods can be thought of as being related to those associated with Ward identities in that they relate vertex corrections to self-energies. However, unlike Ward identities, they have quite general applicability and can be used when Ward identities cannot. Vertex corrections *are* related to quantities that have the appearance of a self-energy, usually though there is no corresponding single-particle self-energy. (In connection with Ward identities, see in particular Ref. 12, which derives them without taking the limit $\omega\rightarrow 0$ and which therefore, as do the present methods, involve finite differences rather than derivatives of the self-energies.)

It perhaps needs to be emphasized that the methods used in this section deal with two-particle propagators, i.e., with vertex functions, e.g., $\Omega(i\omega_n, i(\omega_n+\omega_0))$, summed over the internal frequency ω_n. As a result the only frequency argument is $i\omega_0$ and the poles of the propagator occur in the complex plane associated with this variable. Thus although the single-particle self-energies are functions of either $i\omega_n$ or $i(\omega_n+\omega_0)$, and vertex parts are functions of both, the resulting two-particle self-energy is a function of only the single variable $i\omega_0$.

Consider specifically the spin-spin correlation function. This is obtained by evaluation of the two d-electron vertex function $\Omega(i\omega_n, i(\omega_n+\omega_0))$ shown in Fig. 10. With the frequency labels shown in this figure, the correlation function is given by performing a sum upon ω_n. (For mathematical convenience, in what follows this sum will be implied and repeatedly this dummy variable will be interchanged with the other similar variables involved in the summation over internal frequencies.) To $O(J)$ this transverse correlation function is

$$\chi^0(i\omega_0)=(g\mu_B)^2[(n_{d\uparrow}-n_{d\downarrow})/(i\omega_0-h)] .$$

It has a pole at $i\omega_0=h$. The idea behind defining a two-particle self-energy is to look for repeatable inclusions for the corresponding propagator which will modify the position of this pole. Clearly, the single-particle self-energies are such quantities. In addition are vertex corrections such as those shown in Fig. 11. Vertex corrections are more complicated because they have four rather than two external lines, and therefore are a function of two frequencies, i.e., the two frequencies of the external lines of the vertex on the right-hand side of the diagram. Explicit expressions will be found below.

There are three important identities. First, when the vertex corrections are omitted, and without using the convention that there is a sum on ω_n, Dyson's equation can be written in its two-particle form as follows:

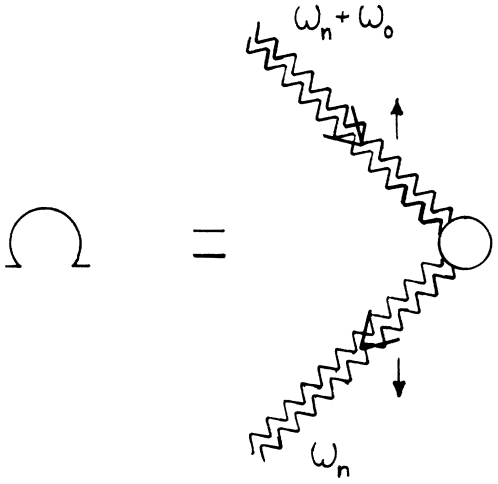

FIG. 10. Vertex which gives the transverse susceptibility. When summed over the external frequency ω_n this will be referred to as a two-particle propagator.

$$\Omega(i\omega_n,i(\omega_n+\omega_0))=(i\omega_0-h)^{-1}\{1-[\Sigma_\uparrow(i(\omega_n+\omega_0))-\Sigma_\downarrow(i\omega_n)]\Omega(i\omega_n,i(\omega_n+\omega_0))\}\ , \tag{4.1}$$

which is trivial to prove. Second, the vertex corrections can be accommodated in a similar identity when use is made of the sum on ω_n. After relabeling the internal sums there is a two-particle equivalent of Dyson's equation *including vertex corrections:*

$$\Omega(i\omega_n,i(\omega_n+\omega_0))=(i\omega_0-h)^{-1}\{1-[\Sigma_\uparrow(i\omega_0,i(\omega_n+\omega_0))-\Sigma_\downarrow(i\omega_0,i\omega_n)]\Omega(i\omega_n,i(\omega_n+\omega_0))\}\ . \tag{4.2}$$

Notice the quantities Σ in this expression now have two frequency arguments as stated earlier. A given vertex correction can always be accommodated in this form after repeated partial fraction expansions.

Consider, by way of example, the $O(J^3)$ bare vertex correction shown in Fig. 11. If, initially, the external lines are taken to be also bare, this corresponds to an expression:

$$\sum_{\omega_n,\omega_{n'},\omega,\omega''}[i(\omega_n+\omega_0)-(h/2+\lambda)]^{-1}[i(\omega_n+\omega_0-\omega+\omega'')-(-h/2+\lambda)]^{-1}$$
$$\times[i\omega_n-(-h/2+\lambda)]^{-1}(i\omega-\varepsilon_{k\uparrow})^{-1}[i(\omega_n+\omega''-\omega_n')-\varepsilon_{k'\downarrow}]^{-1}(i\omega''-\varepsilon_{k''\downarrow})^{-1}\Omega(i(\omega_n'+\omega_0),i\omega_n')\ .$$

The first step is to partial fraction expand the two external impurity propagators which carry the frequencies $\omega_n+\omega_0$ and ω_n. The result is

$$(i\omega_0-h)^{-1}\sum_{\omega_n,\omega_{n'},\omega,\omega''}\{[i(\omega_n+\omega_0)-(h/2+\lambda)]^{-1}-[i\omega_n-(-h/2+\lambda)]^{-1}\}$$
$$\times[i(\omega_n+\omega_0-\omega+\omega'')-(-h/2+\lambda)]^{-1}(i\omega-\varepsilon_{k\uparrow})^{-1}$$
$$\times[i(\omega_n+\omega''-\omega_n')-\varepsilon_{k'\downarrow}]^{-1}(i\omega''-\varepsilon_{k''\downarrow})^{-1}\Omega(i(\omega_n'+\omega_0),i\omega_n')\ .$$

The frequency sums for the term involving propagator $[i(\omega_n+\omega_0)-(h/2+\lambda)]^{-1}$ in the curly brackets are now easy to perform with a result corresponding to Fig. 12(a):

$$\Sigma(i\omega_0,i(\omega_n+\omega_0))=-(J/N)^3\sum_{k,k',k''}\frac{(1-n_k)(1-n_{k''})}{i\omega_0-(\varepsilon_{k''}-\varepsilon_{k'}+h)}\frac{n_{k'}}{i(\omega_n+\omega_0)-(\varepsilon_k-\varepsilon_{k'}+\lambda-h/2)}\ , \tag{4.3a}$$

where the relevant prefactor has been included but the conduction-electron spin labels have been dropped for clarity.

The second term involving the propagator $[i\omega_n-(-h/2+\lambda)]^{-1}$ is a little more difficult to evaluate. The easiest way to proceed is to note, because of the Abrikosov projection, that only the poles of the conduction electrons contribute. This enables the ω and ω'' sums to be performed immediately. The result is

$$(i\omega_0-h)^{-1}\sum_{\omega_n,\omega_{n'}}[i\omega_n-(-h/2+\lambda)]^{-1}[i(\omega_n+\omega_0)-(\varepsilon_k-\varepsilon_{k''}-h/2+\lambda)]^{-1}$$
$$\times[i(\omega_n-\omega_{n'})-(\varepsilon_{k'}-\varepsilon_{k''})]^{-1}\Omega(i(\omega_n'+\omega_0),i\omega_n')\ ,$$

where both the spin labels on the energies and the conduction-electron thermal factors have now been dropped. Now the sum on ω_n can be performed:

$$(i\omega_0-h)^{-1}\sum_{\omega_{n'}}[i\omega_n'-(\varepsilon_{k''}-\varepsilon_{k'}-h/2+\lambda)]^{-1}[i(\omega_n'+\omega_0)-(\varepsilon_k-\varepsilon_{k'}-h/2+\lambda)]^{-1}\Omega(i(\omega_n'+\omega_0),i\omega_n')\ .$$

With a change of summation variable, $\omega_{n'}\to\omega_n$, and with one more expansion this is of the form to fit in Eq. (4.2). With this last expansion the result can be interpreted in terms of the diagrams of Figs. 12(b) and 12(c), i.e., dropping the prefactor of $(i\omega_0-h)^{-1}$ but again including the prefactor of the coupling constant, etc., and corresponding to Fig. 12(b) is

$$\Sigma(i\omega_0,i(\omega_n+\omega_0))=-(J/N)^3\sum_{k,k',k''}\frac{(1-n_k)(1-n_{k''})}{i\omega_0-(\varepsilon_k-\varepsilon_{k''})}\frac{n_{k'}}{i(\omega_n+\omega_0)-(\varepsilon_k-\varepsilon_{k'}+\lambda-h/2)}\ , \tag{4.3b}$$

while for Fig. 12(c) it is the expression

$$\Sigma(i\omega_0,i\omega_n)=-(J/N)^3\sum_{k,k',k''}\frac{(1-n_k)(1-n_{k''})}{i\omega_0-(\varepsilon_k-\varepsilon_{k''})}\frac{n_{k'}}{i\omega_n-(\varepsilon_{k'}-\varepsilon_{k''}+\lambda)}\ . \tag{4.3c}$$

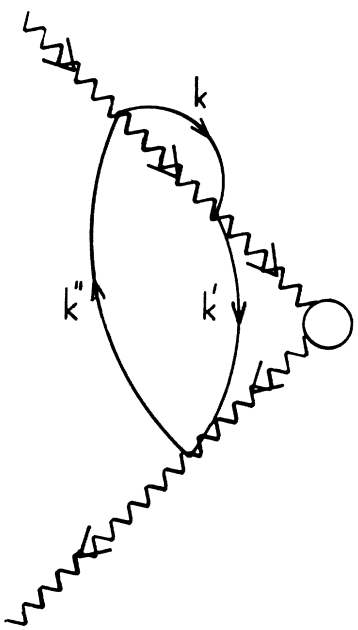

FIG. 11. Bare $O(J^3)$ vertex correction to be evaluated. An important result is that such vertex corrections to a two-particle propagator are fully equivalent to a series of two-particle self-energies corresponding to different time orderings of the vertices. The three significant time orderings for this vertex correction are shown in the next figure.

The first energy denominator, e.g., corresponds to the intermediate state energy between the first and second vertices.

The contributions to the quantities Σ in Eq. (4.3) are not yet two-particle self-energies. These are defined *after* the frequency sum upon ω_n has been performed.

This example contains all of the essential complications to be found in higher-order vertex corrections, including the dressed equivalent of this particular correction. It is always possible, in principle, by the use of repeated partial fraction expansions to reduce a given vertex correction to the form required for Eq. (4.2). Of course with increasing order it rapidly becomes prohibitive to actually do the detailed calculations. That is why it is important that each contribution is in one-to-one correspondence with some time ordering of the interaction vertices. As will be discussed below, this permits the result to be written down by rule of thumb.

As noted in connection with the Abrikosov method for the Anderson model,[6] the thermal factors are easy to determine. Because of the Abrikosov projection, the only thermal factors are associated with the conduction electron lines. The frequencies of these lines are labeled in such a way that the frequency within each impurity line involves sums rather than differences of these same frequencies. The sign of the electron frequency label then determines whether the factor is n_k or $1-n_k$. From this the following rule is deduced: The end of a conduction-electron line is its right-most vertex. If the end is on the top line and the arrow is directed towards the vertex, the thermal factor is $1-n_k$ and n_k for the opposite direction. For the bottom line the rule is reversed. Here the top impurity line runs without kinks from left to right, the bottom line from right to left. Various diagrams up to fourth order have been evaluated both for this and the Anderson model[6] to confirm this rule. Notice that, for example, the three different time orderings of the vertex correction shown in Fig. 12 all have the same thermal factors.

The third identity is obtained by performing the frequency sum on ω_n, which involves the product of the vertex function Ω and a self-energy Σ. The resulting general rule is again best illustrated by example. Corresponding to the second time ordering of the vertex correction, i.e., Fig. 12(b), we have

$$\Sigma(i(\omega_n+\omega_0))\Omega(i(\omega_n+\omega_0),i\omega_n)=\Sigma(-h/2+\lambda+i\omega_0)\Omega(i(\omega_n+\omega_0),i\omega_n)-\Xi(i\omega_0)$$
$$+\Sigma^{ov}(i(\omega_n+\omega_0))\Omega(i(\omega_n+\omega_0),i\omega_n)\ . \tag{4.4}$$

This is obtained by first exhibiting the external lines associated with the vertex:

$$\Omega(i(\omega_n'+\omega_0),i\omega_n')=[i(\omega_n+\omega_0)-(h/2+\lambda)]^{-1}[i\omega_n-(-h/2+\lambda)]^{-1}(1+\cdots) \tag{4.5}$$

then another partial fraction expansion is performed between the last denominator in (4.3b) containing the argument $i(\omega_n+\omega_0)$ and $[i\omega_n-(-h/2+\lambda)]^{-1}$ which corresponds to an external line to Ω.

The quantity $\Sigma(-h/2+\lambda+i\omega_o)$ *is a two-particle self-energy.* Explicitly corresponding to Fig. 12(b) is

$$\Sigma(i\omega_0)=-(J/N)^3\sum_{k,k',k''}\frac{(1-n_k)(1-n_{k''})}{i\omega_0-(\varepsilon_k-\varepsilon_{k''})}\frac{n_{k'}}{i\omega_0-(\varepsilon_k-\varepsilon_{k'})}\ . \tag{4.6}$$

The two denominators of this self-energy can be inferred by taking the two vertical cuts shown in the figure. The simple argument $i\omega_0$ on the left-hand side is used to indicate the quantity defined by Eq. (4.6) is a two-particle self-energy.

The new quantity Ξ *corresponds to an inhomogeneous term.* (It would be an inhomogeous term in the equation-of-motion method.) Following an expansion, it results from the 1 on the right-hand side of (4.5) after the implicit sum is made on ω_n. The inhomogeneous term is in a one-to-one correspondence with Fig. 12(b); it is represented by the diagram in Fig. 13 and the following expression:

$$\Xi(i\omega_0)=-(J/N)^3\sum_{k,k',k''}\frac{(1-n_{k''})}{i\omega_0-(\varepsilon_k-\varepsilon_{k''})}\frac{n_{k'}}{i\omega_0-(\varepsilon_k-\varepsilon_{k'})}\frac{n_k(1-n_{k'})n_\downarrow-(1-n_k)n_{k'}n_\uparrow}{\varepsilon_k-\varepsilon_{k'}-h}\ , \tag{4.7}$$

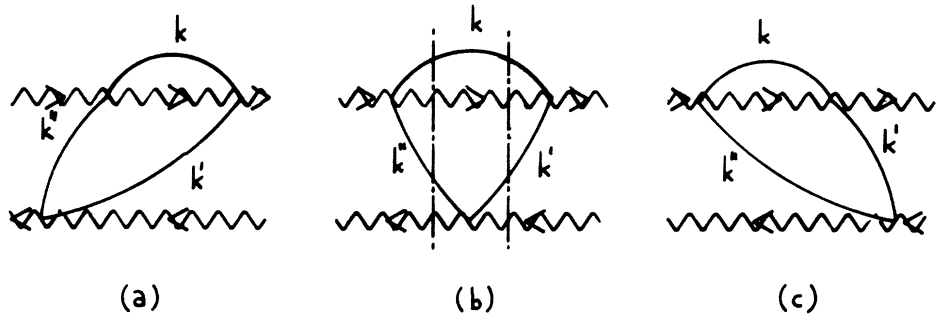

FIG. 12. Three time orderings which correspond to two-particle self-energies. The denominators in each diagram correspond to vertical cut, as shown for (b). The thermal factors can be obtained by rule of thumb as explained in the text. The expression corresponding to (b) is Eq. (4.3) of the text.

which clearly does not contribute to the pole near $i\omega_0=h$. These inhomogeneous terms enter the numerator of the two-particle propagator and will not be needed here. They *are* important to the analytic properties of the propagator, (see Ref. 9).

The thermal factors and denominators in both the two-particle self-energy and inhomogeous term are given by simple rules. It only remains to ascribe a net sign to each contribution. This of course may be done from the sign of the initial diagram by following, in detail, the partial fraction expansions required to obtain this result. However, this process can also be reduced to a rule of thumb which will be given below.

The quantity left in Eq. (4.4), i.e., Σ^{ov} is of higher order in the coupling constant J. These contributions result from the ellipsis on the right-hand side of (4.5) and involve the relabeling of the sums. The beginning vertex correction was $O(J^3)$ and the lowest order to appear in Σ^{ov} will be $O(J^5)$. Mathematically iterating Eq. (4.4) generates a power series for the two-particle self-energy. However, the real usefulness of Eq. (4.4) stems from a diagrammatic interpretation of the new term Σ^{ov} as leading to *overlapping* two-particle self-energies. Figure 14 shows an overlapping contribution involving the vertex of Fig. 12(b) and an $O(J^2)$ single-particle self-energy. Figure 9(a) shows an $O(J^4)$ overlapping contribution from two $O(J^2)$ single-particle self-energies. Such time orderings of the vertices have an obvious physical meaning. The thermal factor is the product of those for the two parts; the energy denominators are again obtained by taking vertical cuts through the diagram and the net sign by a second rule of thumb to be given below. The corresponding inhomogeneous terms can be obtained by these same rules by allowing overlap of self-energies with the elementary inhomogeneous terms.

These overlapping terms are not individually negligible. For example, the overlapping diagram of Fig. 9 is fully equivalent to an $O(J^2)$ vertex correction of the form shown in Fig. 1(a) and discussed in the Introduction. The cancellation of such terms is important and will be discussed in the next section.

The net sign of a two-particle self-energy is determined by the sequence of partial fraction expansions required to put every energy denominator in the following form:

$$i\omega_0-(\text{some sum and difference of energies})\,. \tag{4.8}$$

For the $O(J^3)$ single-particle self-energy of Fig. 15(a) this requires two expansions against the bare down d-electron propagator. The sign of the term retained as the direct (rather than the beginning of an overlapping) self-energy therefore has a factor $(+1)^2$. On the other hand, the mirror-image self-energy, Fig. 15(b), has a factor $(-1)^2$ because of similar expansions with the, top, up-spin line, but begins with a negative sign in Eq. (4.1), and so has

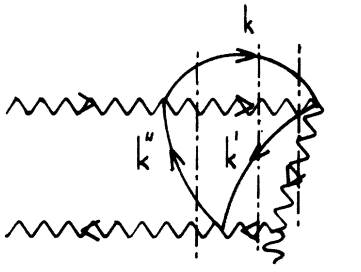

FIG. 13. Inhomogeneous term corresponding to the exemplified two-particle self-energy of Fig. 12(b). The relevant expression is Eq. (4.5). Such terms are fully equivalent to inhomogeneous terms in the equation-of-motion method and are an essential feature of two-particle propagators. Notice the external vertex indicated by the wiggly tail at the bottom right of the figure.

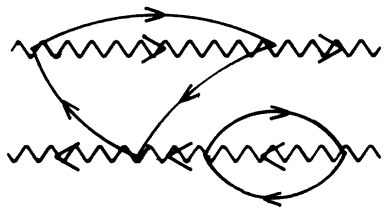

FIG. 14. The simplest overlapping diagram generated by the exemplified $O(J^3)$ two-particle self-energy. This diagram is fully equivalent to an $O(J^2)$ vertex correction of the extreme right-hand vertex of the $O(J^3)$ term.

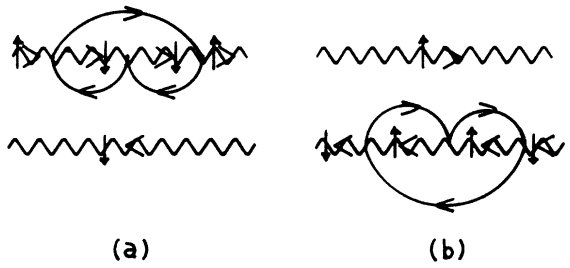

FIG. 15. Two mirror-image two-particle self-energies which illustrate the factors which determine the net sign of a contribution. Starting from the single-particle self-energy (a) involves two partial fraction expansions with the bottom line. This gives a factor of $(+1)^2$. In contrast (b) requires two expansions against the top line which introduces a factor $(-1)^2$. In addition, this term started with a minus sign in Eq. (4.1) or (4.2) and so has a net opposite sign to its mate.

net negative sign relative to its mate. If only one elementary vertex is transferred to the lower line [Fig. 12(a)] to form a vertex correction, then it is easy to show the corresponding contribution is equal in magnitude to that from a single-electron self-energy shown in Fig. 15(a), except the sign is opposite. The sign of other more complicated vertex corrections, etc. can be deduced by inductive reasoning. The result is a factor,

$$(-1)^{n_e},$$

where n_e equals the number of conduction-electron lines which end on the bottom line, and where the meaning of a line ending is the same as in the above. This rule implies that all of the two-particle self-energies [Fig. (12)] resulting from a single vertex correction have the same net sign.

The present approach would be prohibitive without these prescriptions used for the direct evaluation of the relevant two-particle self-energies and for the estimation of omitted contributions.

The method for defining two-particle self-energies and inhomogeneous terms is unique. In the same way as Dyson's equation defines a single-particle self-energy, mathematically the two-particle self-energies and the associated inhomogeneous terms are defined by the following which explicitly displays the sum on ω_n:

$$\sum_{\omega_n}[\Sigma_\uparrow(i\omega_n+i\omega_0)-\Sigma_\downarrow(i\omega_n)]\Omega(i(\omega_n+\omega_0),i\omega_n)$$
$$=\Sigma(i\omega_0)\sum_{\omega_n}\Omega(i(\omega_n+\omega_0),i\omega_n)-\Xi(i\omega_0)\,, \quad (4.9)$$

where again the simple argument ω_0, and the lack of a subscript on the right-hand side, indicates $\Sigma(i\omega_0)$ is the two-particle self-energy. The sequence of partial fraction expansions and the division into self-energies and inhomogeneous terms is fixed by the requirement that the denominators of the self-energies be of the form $i\omega_n-$(an energy). In terms of diagrams this self-energy is defined as a repeated inclusion in a two-particle diagram. Typical such inclusions are illustrated in Figs. 9, 12, 14, and 15, while all $O(J)$ and $O(J^2)$ such diagrams are shown in Fig. 16. The inhomogeneous terms are true vertex corrections in that they appear in the numerator of the propagator; diagrammatically, each corresponds to the overlap of some two-particle self-energy with an external vertex as illustrated by Fig. 13. They have the characteristic of not having any poles near those of the two-particle propagators. In fact, in the present application they have cuts rather than isolated poles. The same method has quite general applicability; however, when applied to, e.g., the conduction-electron susceptibility the scheme becomes more involved; see Ref. 9. The method can also be applied to problems where coupled vertex equations occur; again, see Ref. 9.

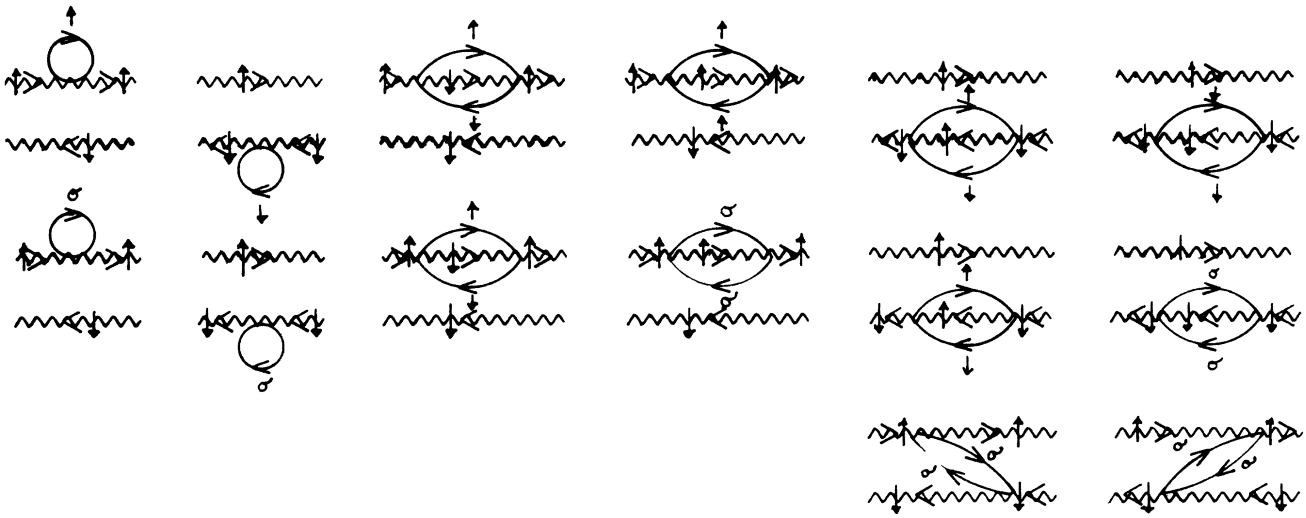

FIG. 16. Illustrated are all $O(J)$ and $O(J^2)$ two-particle self-energies. The bottom two lines correspond to the standard Abrikosov representation which as compared to the nonstandard version has two vertex corrections shown in the last line. Since the results for a physical quantity cannot depend upon the representation, the total of the longitudinal diagrams, i.e., vertex corrections and self-energies, in one case must be exactly equal to the self-energies alone for the nonstandard method. This illustrates that two-particle self-energies which arise from single-particle self-energies and vertex corrections are equivalent and must be treated on an equal footing.

V. SELF-CONSISTENT PARQUET APPROXIMATION

The aim of the present approach is to obtain a self-consistent equation which corresponds roughly to the usual equation of the scaling theories. In a diagram theory attention is usually focused upon the evaluation of the relevant self-energy(ies). While as mentioned in the Introduction the only well-defined self-energy is that of the two-particle propagators and, in particular, that of the transverse susceptibility. The purpose of this section is to therefore derive a suitable self-consistent equation for this quantity. Specifically, what is considered is the self-consistent evaluation of the two-particle self-energy, as defined in the preceding section, put on its energy shell using the kink method described in Sec. III. This same two-particle self-energy invariably appears as dressing in the diagram prescription for the various other quantities which are to be evaluated in the present approach. It is therefore a quantity of fundamental interest.

The impurity transverse susceptibility gives information about transitions between the (often much renormalized) $S_z=\frac{1}{2}$ to $-\frac{1}{2}$ states of the impurity. There is a pole of the susceptibility corresponding to the energy for each such transition. If such a pole has no width it corresponds to the exact energy difference between the two eigenstates of the system with these spin values.

Results for this susceptibility in the perturbation limit appeared in the literature on ESR in dilute alloys well over a decade ago.[9,16,17] The results of such calculations are in agreement with the expectations of scaling theory.[15]

The leading $O(J)$ and $O(J^2)$ diagrams in both the standard and nonstandard Abrikosov representations are shown in Fig. 16. A comparison between the two diagram prescriptions is instructive since with the standard technique there is an $O(J^2)$ vertex correction while the alternative approach gives none. This appropriately illustrates that vertex corrections for the impurity are just another form of two-particle self-energy. On energy shell, at zero temperature, the longitudinal terms do not contribute. The transition energy is

$$g\mu_B H(1+\rho J_{\text{eff}}/2)\ , \tag{5.1}$$

and the width is

$$\tfrac{1}{2}\pi(\rho J)^2 g\mu_B H\ , \tag{5.2}$$

where $J_{\text{eff}}=J[1+\rho J\ln(g\mu_B H/\tilde{D})]$ is the usual expression, to $O(J^2)$, for the effective exchange. Higher-order terms will renormalize the exchange in the width formula. In fact, the width can be incorporated in the energy formula by giving the logarithm a suitable imaginary part:

$$\ln(g\mu_B H/\tilde{D})\rightarrow\ln(g\mu_B H/\tilde{D})+i\pi/2\ .$$

As stated in the Introduction, not only do the longitudinal self-energies not contribute to the low-order perturbation expansion, the purely longitudinal diagrams do not contribute, on energy shell, to the logarithmic divergences in any order. This follows from particle-hole symmetry. It is easy to show that the sum of a given diagram plus that obtained by reversing the direction of the conduction-electron lines is at most $O(H^2)$.

The purely longitudinal diagrams, beyond $O(J)$, therefore can be taken as a skeleton set, the sum of which is not logarithmic divergent in any order. However, it would be dangerous to throw away the longitudinal diagrams or more particularly the dressed version of these diagrams without some more-detailed consideration. The dressing of the vertices of the longitudinal series begins by the replacement $L\rightarrow TT$, which when added to the bare L vertex leads to an effective longitudinal interaction J_{eff} specified above. Including higher-order corrections leads to the usual logarithmic series for J_{eff}, implying the vertex in the longitudinal series has a value of order unity for a cutoff of the order of $4\pi T_0$. It would appear that such a large longitudinal interaction, even though it still generates no logarithmic terms, cannot be ignored since at first sight it is capable of grossly modifying the wave functions in the vicinity of the impurity and, through this, modifies in turn the effective vertex.

This raises the difficult question of vertex corrections. It is well known that the vertex corrections are the relevant diagrams required to account for the above renormalization of the wave function, and it is also known that the vertex correction shown in Fig. 17(a) is the one which generates the $|\rho J|^{1/2}$ factor in T_H and must be included. However, it is also well known that, at least in the weak limit, this factor arises within the self-consistent parquet approximation. Indeed the self-consistent nature of the approximation does include all vertex corrections of the form of Fig. 17(b) where bubbles lie within bubbles.

With the nonstandard version of the Abrikosov representation there are no overlapping bubble on bubble diagrams of the structure shown in Fig. 17(c), except the purely $LLLL$ term which is not needed. There is always one or more vertices in the combinations $TTTT$, $TLTL$, and $LTLT$ which are not allowed. In contrast, for the traditional version of the representation, $TLTL$ and $LTLT$ diagrams do exist. Again this illustrates the nonunique nature of the d-electron single-electron self-energy. It also illustrates that there is a cancellation of vertex corrections against self-energies in both representations. While there are no single-particle diagrams of this kind, there are overlapping two-particle vertex corrections of this structure as illustrated in Figs. 18(a) and 18(b). The pairs vertically above each other cancel. Other vertex corrections arising from overlapping self-energies also cancel. However, this is nontrivial in that longitudinal corrections are compared with their transverse counterparts and some dressings of self-energies are involved. This will be discussed later in this section and in an appendix. While these overlapping bubble vertex corrections cancel, other vertex corrections such as that in Fig. 11 do *not* cancel. As will be seen below, there are many such vertex corrections in the parquet series which is summed. Also, the vertex corrections discussed by, e.g., Coleman[5] in connection with the author's[6] method for the Anderson model *are* important. Here, the equivalent of those diagrams generate part of the parquet series. Further discussion of these vertex corrections will be found later in this section.

The diagrams are therefore classified into two groups: (i) the $O(J)$ longitudinal diagram with a dressed vertex

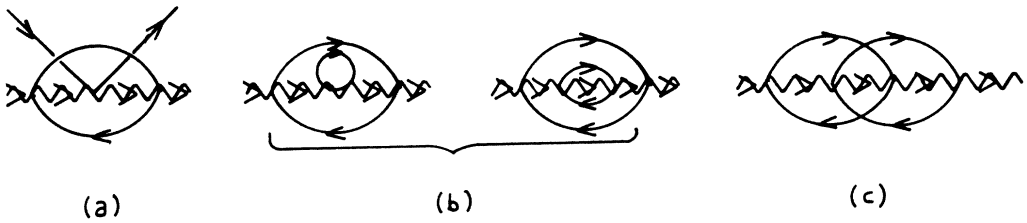

FIG. 17. The elemental vertex correction illustrated in (a) can be viewed as generating both the bubble inside bubble dressings of the self-energies, examples of which are shown in (b), in addition to true vertex corrections of which the first is illustrated in (c).

and (ii) higher-order longitudinal diagrams with dressed vertices. These latter diagrams can be neglected.

The aim is to smoothly connect the large-to-small cutoff self-energy for the problem. Because the two-particle self-energy is placed on its energy shell the effective cutoff is the magnetic field rather than the customary energy.

In fact, it is rather obvious that the weak- and strong-coupling limits can be smoothly coupled when the cutoff is the magnetic field, but not so if it is the energy. The ground state of the problem consists of a spin singlet $S=0$ which has a binding energy of order $4\pi T_0$. The action of S^+ will be to create an excited triplet state $S=1$. Such a spin flip must therefore cost an energy of the order of the binding energy of the singlet, i.e., there is a gap of order T_0 separating the ground state from excited states *of the impurity*. As will be shown explicitly in Sec. X, this does *not* imply there is a gap in the conduction-electron excitation spectrum. (A similar situation exists for a gapless superconductor; the binding energy for pairs is finite even in the absence of gap in the conduction-electron spectrum.) Also, it might be noted that there can be no strict gap in the impurity spectrum at nonzero temperatures. (This impurity spectrum cannot be calculated directly by the Bethe methods.)

The impurity ground-state-energy scheme must look something like the left-hand side of Fig. 19. There will be a finite self-energy for the spin-spin correlation function corresponding to a transition from the ground state to the excited state marked with the arrow labeled 1. For increasing energies ϵ (and zero field) this branch of the self-energy corresponds to transitions like that indicated by arrow 2 which end in the continuum of decaying excited states. However, it is clear that however large the energy, the self-energy for this branch necessarily involves the ground-state energy $4\pi T_0$, which of course cannot be expressed as a power series in ρJ. Thus the ground-state self-energy cannot be connected to the usual perturbation expansion for large energies. Increasing the field breaks up the singlet and changes the nature of the ground state. Therefore for large fields the energy scheme appears as on the right-hand side of Fig. 19. A relevant self-energy would have a value corresponding to the transition marked by arrow 3. Since this energy does have an expansion in ρJ it is possible that a single branch of the self-energy as a function of field can be used to connect the large-field, weak-coupling limit to the small-field, strong-coupling or ground-state limit.

The idea is then to classify diagrams as to types (i) and

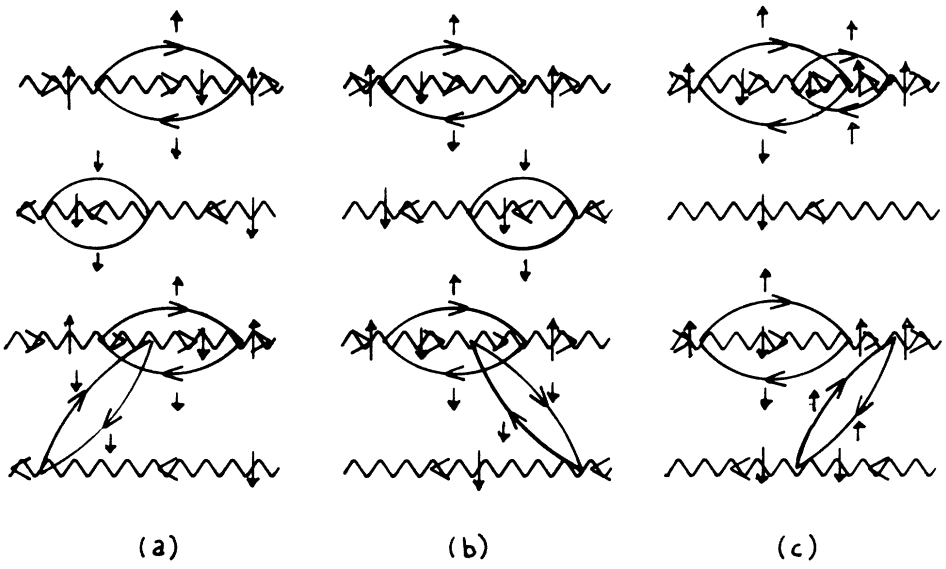

FIG. 18. Illustrated are two-particle self-energies which are equivalent to the type of single-particle vertex correction illustrated in Fig. 1(a). The pairs vertically above each other cancel. Transferring one vertex from the top to the bottom line changes the sign if both lines have the same spin label. The pair (c) only exists for the standard representation.

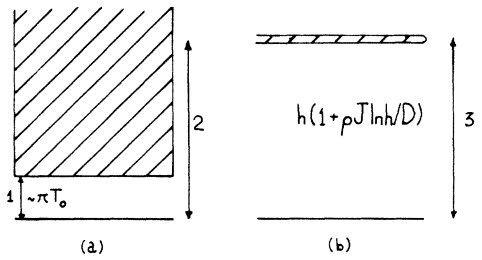

FIG. 19. The energy-level scheme for the ground state in zero field must be something like that illustrated in (a). There is the isolated singlet ground state an energy of order T_0 below the continuum. Both the low-energy transition 1 and the higher-energy transition 2 involve T_0, and therefore have an energy which is not given by an expansion in the exchange J. In contrast, the high-field ground state has an energy-level scheme as in (b). The transition marked 3 does correspond to an expansion in J. It is implied that the high-field expansion and the ground state can be connected while the high-energy expansion cannot.

(ii) discussed above. All two-particle self-energies, as defined in the preceding section, up to $O(J^3)$ are shown in Fig. 20. In general, diagrams will contain a mixture of intermediate-state denominators, some with the "longitudinal" cutoff $h-\varepsilon$ and others the "transverse" ε. All diagrams which are purely transverse are of type (i) and correspond to a dressing of the $O(J)$ vertex, while the others are of type (ii) and can be viewed as dressings of the purely longitudinal skeletons. Again the latter are negligible.

Two purely transverse sets of diagrams have been identified: Those in Fig. 21(a) can be associated with the upper line, while those in Fig. 21(b) can be taken to correspond to the lower line. Characteristics of both sets are the same: the extreme end vertices are both transverse while those in the middle are all longitudinal. There is a single conduction-electron line connecting the two end vertices. The expression corresponding to the sum of these diagrams is easily obtained by the rules of the preceding section. Consider the diagram in Fig. 20(a), all vertices are attached to the top line. Corresponding to the single conduction line parallel to the impurity line is a thermal factor $(1-n_k)$, while for each of the antiparallel lines there is a factor $n_{k'}$, $n_{k''}$, etc. However, when one of the intermediate longitudinal vertices is transferred to the bottom line, to give Fig. 20(b) its factor $n_{k''}$ changes to $1-n_{k''}$ and there is a change of sign corresponding to one conduction-electron line finishing on the bottom line. As a result transferring such a vertex generates another contribution with a leading logarithmic divergence of the net same sign.

Rather than writing a result for the total self-energy itself, it is more convenient to give the sum in terms of a differential. Consider again the simple $O(J^3)$ diagram of Fig. 20(a); writing the sums over momentum as integrals gives the following contribution:

$$\Sigma(\varepsilon)=(\rho J/2)^3\int_0^D d\varepsilon'\int_{-D}^0 d\varepsilon''\int_{-D}^0 d\varepsilon'''\frac{1}{\varepsilon-(\varepsilon'-\varepsilon'')}\times\frac{1}{\varepsilon-(\varepsilon'-\varepsilon''')}\,, \tag{5.3}$$

where the expression has been continued to the real axis $i\omega_0\to\varepsilon$. The Zeeman energy $g\mu_B H$ should, in general, appear in the large energy cutoff $\pm D$ for each integral. The approximation of ignoring these corrections to the ultraviolet cutoff is not negligible; the exact evaluation of the crossover ratio W' requires that a careful accounting be made of these approximations. Here approximations of this type will be freely made. An accounting will be found in Sec. VII. Using such an approximation, the argument can be shifted into the lower limit of the first integral:

$$\Sigma(\varepsilon)=(\rho J/2)^3\int_{-\varepsilon}^D d\varepsilon'\int_{-D}^0 d\varepsilon''\int_{-D}^0 d\varepsilon'''\frac{1}{\varepsilon'-\varepsilon''}\frac{1}{\varepsilon'-\varepsilon'''}\,. \tag{5.4}$$

It is important to notice that when manipulated in this way, the self-energy Σ is a function of ε only. The field only appears explicitly when the self-energy is put on its energy shell, i.e., when approximately $\varepsilon=h$. [Recall $h=(1+\frac{1}{2}\rho J)g\mu_B H$ includes the $O(J)$ correction.] The

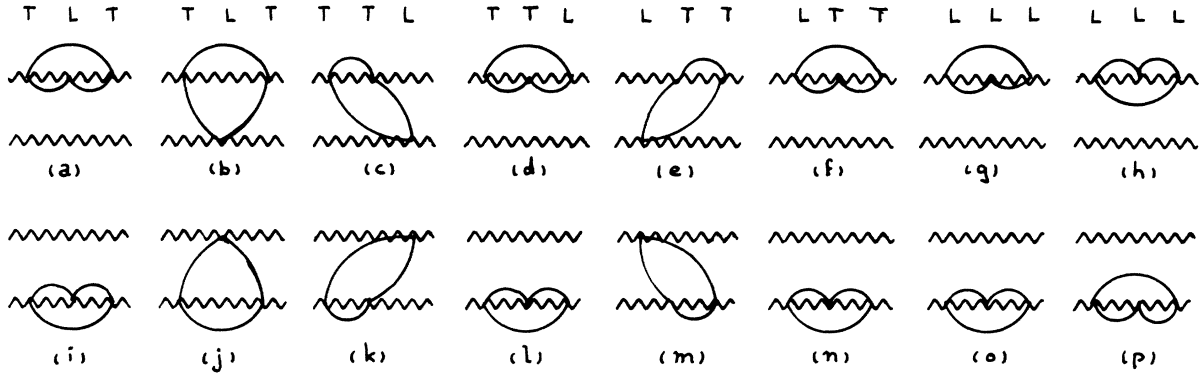

FIG. 20. Totality of two-particle self-energies in $O(J^3)$. A single vertex correction generates, e.g., all three time orderings (b), (c), and (e). The contributions (a), (b), (i), and (j) are those which generate the leading parquet approximation. The other contributions are discussed in the text. The letter L or T denotes the type of vertex, longitudinal or transverse, respectively.

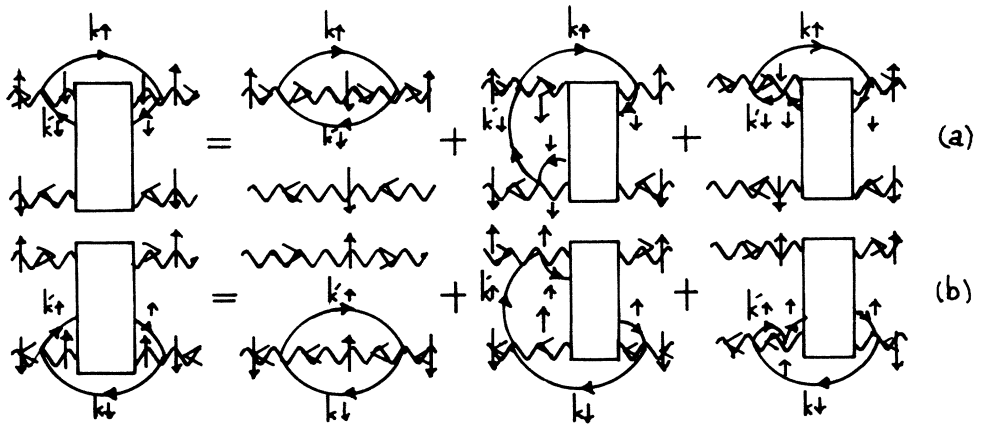

FIG. 21. (a) The purely transverse diagrams which are associated with the upper line. (b) The mirror-image diagrams associated with the lower line. The full series is obtained by iterating this diagram. As discussed in the text, it is this series which generates the important leading parquet approximation.

$O(J)$ two-particle self-energy $\frac{1}{2}\rho Jh$, however, *is* explicitly a function of h and does not conform to the same pattern. It will turn out that for this reason it must be accounted for separately. The desired result for now is obtained with $\varepsilon=h$ by differentiating with respect to the field h:

$$\frac{d\Sigma}{dh}=(\rho J/2)^3\int_{-D}^{0}d\varepsilon'\int_{-D}^{0}d\varepsilon''\frac{1}{h-(\varepsilon-\varepsilon')}\frac{1}{h-(\varepsilon-\varepsilon'')}$$
$$=\left[(\rho J/2)\int_{-D}^{0}d\varepsilon'\frac{1}{h-(\varepsilon-\varepsilon')}\right]^2. \tag{5.5}$$

The result is similar for each term in the leading logarithmic series, Fig. 21. Differentiation with respect to the field leaves a power series in the logarithmic integrals for $d\Sigma/dh$. Before writing down the result, the calculation is made self-consistent.

Because of the single-loop rule, the conduction-electron lines within a self-energy cannot have self-energy inclusions. The dressing of the self-energy comes about from including two-particle self-energy inclusions on the antiparallel, longitudinal lines within the diagram. This can be done by the straightforward extension of the rules devised for the self-energy itself.

The last important step in the evaluation of the parquet approximation is to put the two-particle self-energy on its energy shell by the partial fraction expansion, or kink, method described in Sec. III. In general terms, the transverse susceptibility is of the following form:

$$\frac{N}{i\omega_0-\Sigma(i\omega_0)-h}\,. \tag{5.6}$$

The numerator N is just a prefactor and is not involved in the determination of the poles of the susceptibility. The problem of determining approximation schemes for the energy shell for $[i\omega_0-\Sigma(i\omega_0)-h]^{-1}$ is almost identical to that for the single propagators considered in Sec. III. One begins by taking the first partial fraction expansion between the rightmost denominator of the two-particle self-energy and the bare two-particle propagator immediately to the right. With the kink prescription this generates odd-looking diagrams for the kink self-energy such as those shown in Fig. 22. One has a total of four impurity lines in the intermediate state of this kink self-energy. However, the two antiparallel lines indicated by the arrows in this figure come about from bending up the bottom line of the susceptibility bubble and do not contribute to the intermediate-state energy first because the bare energies of the two lines cancel and second because the self-energies associated with these two lines also cancel. The former statement follows from the rule of taking a horizontal cut through the diagram in order to determine the relevant intermediate-state energy. The latter statement is justified in the Appendix.

Thus, the relevant dressing for the intermediate state is that of an antiparallel opposite spin pair, which is just the quantity being evaluated. This directly implies the latter quantity must be evaluated self-consistently. However, the situation is a little more complicated than would appear at first sight.

One might reasonably expect that the relevant dressing would consist of the transverse two-particle self-energy, while it turns out that the dressing to be used is purely longitudinal. The intermediate state already involves the Zeeman energy, and any further spin flips would cause this to be canceled, leaving only the frequency as the cutoff. With a longitudinal dressing the intermediate state still has the field as its low-energy cutoff. In turn, the self-energy contained inside this dressing and so on is also purely longitudinal. It is these longitudinal self-energies that make the parquet approximation self-consistent. The fact that this construction correctly reproduces results for the next to leading order parquet approximation, and in particular the famous prefactor of $|\rho J|^{1/2}$, will be evident from the solution of the resulting equations. This provides *a posteriori* confirmation of the present statements.

Justifying the previous few paragraphs *a priori* is rather complicated and involves numerous vertex corrections,

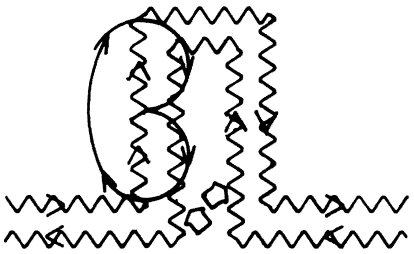

FIG. 22. Illustrated in an $O(J^3)$ kink two-particle "self-energy." The same spin pair of lines indicated by the arrows do not contribute to the intermediate-state energy. When considered together with overlapping contributions the self-energies of these lines are found to cancel.

etc. For the nonstandard Abrikosov method there are no *TLTL* or *LTLT* vertex corrections. However, there are higher-order vertex corrections which correspond to dressings of these taken as skeletons. The fact that the skeletons do not occur in the nonstandard representation simply reflects the fact that they cancel in the standard one. The dressings cancel in both representations.

There are several *TTTT* contributions. These are of two types: first, the omitted transverse dressings and second, four two-particle self-energies which come from the one *TTTT* vertex correction.

There are also overlapping *TLTL*, *LTLT*, and *TTTT*, self-energies both for kink and two-particle quantities. Direct evaluation of such a diagram on the energy shell (see Sec. III) shows that it should be compared with the diagram [Fig. 9(b)] which generates a self-energy correction within the self-energy. Together they give the following contribution:

$$\frac{\partial\Sigma^{(2t)}}{\partial\varepsilon}\Sigma^{(2t)}, \tag{5.7}$$

which is the first term in the Taylor series which would cause the nominal energy shell h to be replaced by its exact value.

The cancellation of these remaining terms is neither exact nor trivial. It involves the cancellation of longitudinal by transverse contributions, and therefore is only valid for an isotropic exchange interaction. This cancellation is correct to the next to leading order approximation which, for the reasons stated in the Introduction, is sufficient. This cancellation is dealt with in the Appendix.

The result of this self-consistent evaluation of the transverse self-energy is

$$\frac{d\Sigma}{dh}=\tfrac{1}{2}\left[\frac{1}{\rho J}-\tfrac{1}{2}(I^{+}+I^{-})\right]^{-1}-\frac{\rho J}{2}, \tag{5.8}$$

where the self-consistent logarithmic integrals are

$$I^{\pm}=\int_0^{\pm D}d\varepsilon\frac{1}{\varepsilon+\Sigma(h-\varepsilon)-h}. \tag{5.9}$$

While the path by which it was obtained might be unfamiliar, the result [Eqs. (5.8) and (5.9)] should be no surprise. Without the self-energy in the denominator the integrals $I\sim\ln(h/D)$, i.e., $d\Sigma/dh+\rho J/2$ is just the usual formula for the renormalized exchange interaction part. The fact that this is the differential of a self-energy may be viewed as some kind of Ward identity, and that the self-energy should appear in a self-consistent way in the integrals makes obvious sense. There are perhaps two features which might be troubling: first, the $\rho J/2$ on the right-hand side of Eq. (5.8) and second that this is an equation for Σ as a function of field, while within the integral the argument of this quantity is really the intermediate-state energy. These two features are related.

The fact that the energy and field arguments are equivalent implies that the two-particle self-energy, before it is put on shell, is a function of ε only. As noted already, this *is* so for all but the $O(J)$ self-energy. The $O(J)$ term must therefore be subtracted out from the right-hand side of (5.8) and, in principle, be accounted for separately; however, in practice it can be ignored in the scaling limit, except in the weak-coupling regime when the integration constant K is evaluated (see Sec. VII). Alternatively, it is not difficult to see that if the $O(J)$ term *were* included in (5.8) the key, next to leading order, $O(J^3)$ contribution would be incorrectly given. [Recall that an $O(J)$ term *is* included in the definition of h.]

What would appear to be similar self-consistent equations for the Anderson model were obtained by Inagaki.[4] However these equations are for a single-particle self-energy, they do not account for vertex corrections, and are *not* equivalent to the present equations even in the $U\rightarrow\infty$ limit.

The last step in deriving a key result is to differentiate again with respect to h. To obtain the following result it is again necessary to ignore an $O(h)$ modification to the high-energy cutoff $\pm D$. Again such approximations are important when considering the high-field or weak-coupling limit; see Sec. VII:

$$(\Sigma-h)\frac{d^2\Sigma}{dh}+2\left[\frac{d\Sigma}{dh}+\frac{\rho J}{2}\right]^2=0. \tag{5.10}$$

If instead the result is written in terms of the full transverse self-energy, i.e., $\Sigma\rightarrow\Sigma+(\rho J/2)h$, and if h is redefined, i.e., $h\rightarrow h[1+(\rho J/2)]$, then

$$(\Sigma-h)\frac{d^2\Sigma}{dh}+2\left[\frac{d\Sigma}{dh}\right]^2=0. \tag{5.11}$$

Equation (5.11) is a universal nonlinear differential equation for the two-particle impurity self-energy, i.e., it depends on neither the bare cutoff nor the bare coupling constant. It should be considered as a generalization of the usual scaling laws for this problem; the relation to which will be discussed in the next section. This equation is the principle result; the rest of this paper will be largely a study of the properties of solutions to this equation.

VI. RELATION TO CONVENTIONAL SCALING

Although, at first sight, Eq. (5.11) does not appear to be simply related to the conventional scaling equations, a simple change of variables reduces it to a familiar form. These steps are also required for the first integration of

this differential equation.

First though recall the following simple way to obtain the standard scaling law.[18] In the present notation the effective exchange constant within perturbation theory is

$$\rho J_{\text{eff}} \equiv 2g = \rho J + (\rho J)^2[1+\tfrac{1}{2}(\rho J)]\ln(h/D) + \cdots . \quad (6.1)$$

As is well known the leading logarithmic term arises from the diagram shown in Fig. 3(a), while the displayed $O(J^3)$ term corresponds to the vertex shown in Fig. 17(a). Equivalently the impurity self-energy in the leading approximation corresponds to Fig. 3(a) while the $O(J^3)$ term appears when this term is evaluated self-consistently.

The usual scaling equation is obtained by removing an infinitesimal strip dD from the top and bottom of the conduction-electron bands. The change dg in the exchange (recall $2g=\rho J_{\text{eff}}$ in a more standard notation) is obtained from Eq. (6.1):

$$\frac{dg}{dD} = 2\left[\frac{1}{D}\right] g^2(1+g+\cdots) . \quad (6.2)$$

With the definition $y=\ln(D/D_0)$ this becomes

$$\frac{dg}{dy} = 2g^2(1+g+\cdots) . \quad (6.3)$$

A similar equation is obtained from Eq. (5.11) by the substitutions $Z=\Sigma-h$ and $g=d\Sigma/dh$ to give

$$Z(g-1)\frac{dg}{dZ} = -2g^2 . \quad (6.4)$$

With $y=\ln(Z/D)$ this is comparable with Eq. (6.3):

$$\frac{dg}{dy} = 2g^2/(1-g) . \quad (6.5)$$

Apart from the different cutoff used, these equations agree for the weak-coupling limit when $g \ll 1$ and $h \gg \Sigma$. Also, in this form, the latter equation is trivial to integrate:

$$\tfrac{1}{2}(1/g+\ln g)+\ln[(\Sigma-h)/K]=0 . \quad (6.6)$$

This step introduces the first integration constant K. It has the dimensions of energy and plays the role of energy scale. It is proportional to the Kondo temperature. A precise value will be obtained in the next section by comparison with the high-field or weak-coupling limit.

The rest of this section is concerned with the second integration, although little use will be made of the results. The first step is to solve for Z:

$$Z = Kg^{-1/2}e^{-1/2g} . \quad (6.7)$$

Next is a differentiation with respect to h:

$$g-1 = \frac{dZ}{dh} = -[(g-1)/2g^2]Kg^{-1/2}e^{-1/2g}\frac{dg}{dh} . \quad (6.8)$$

After some cancellation, with $s=1/2g$, and after integrating,

$$h+a = K\int^{1/2g}(2s)^{1/2}e^{-s}ds . \quad (6.9)$$

The integral is that for an incomplete γ function of power $\frac{3}{2}$, so the final result in closed form is Eq. (6.6) with

$$h+a = 2^{1/2}K\gamma(\tfrac{3}{2}, 1/2g) . \quad (6.10)$$

The second integration constant "a" actually corresponds to an autonomous property of Eq. (5.11): Given a solution $\Sigma(h)$ there are a series of solutions $\Sigma(h+a)+a$, since Eq. (5.11) is unchanged by the transformations $\Sigma\to\Sigma+a$ and $h\to h+a$.

VII. WEAK-COUPLING–HIGH-FIELD LIMIT

Taking the first integration of the Eq. (5.11) gives (6.6). This can be rewritten as

$$g = -\frac{1}{2}\frac{1}{\ln(g^{1/2}Z/K)} . \quad (7.1)$$

It is necessary to compare this with the relevant high-field perturbation-theory expression. Some care is required in order to compare it with the correct high-field expansion. As was pointed out in Sec. V, approximations were made to the high-energy cutoff energies in order to obtain the simple result Eq. (5.11). The above must be compared with a high-field expression for which the same approximations have been made. In differentiating the logarithmic integrals they were approximated by, for example,

$$I^+ = \int_{-h}^{D} dx[x+\Sigma(-x)]^{-1} = \int_0^{D+h} d\varepsilon[\varepsilon+\Sigma(h-\varepsilon)-h]^{-1} . \quad (7.2)$$

The point of the approximation is for $dI^+/dh=(\Sigma-h)^{-1}$ exactly; however, in the second line the upper cutoff should clearly be D not $D+h$. To maintain particle-hole symmetry the second-order contribution to the self-energy must be

$$I_2 = (\rho J)^2\int_{-D-h}^{0} d\varepsilon' \int_0^{D+h} d\varepsilon(\varepsilon'-\varepsilon-h)^{-1} \simeq h(\rho J)^2\ln(-h/2eD) . \quad (7.3)$$

Most important is the 2 in the logarithm. If this expression is directly differentiated with respect to the field h, in order to compare it with Eq. (7.1), the 2 remains and so the effective upper cutoff with the present approximations to the standard Kondo model is $2D$ rather than D. Keeping in mind that between Eqs. (5.10) and (5.11) the definitions of $\Sigma(h)$ and h were modified, it is necessary to compare Eq. (7.1) with the following high-field result:

$$g \equiv \frac{d\Sigma}{dh} = \tfrac{1}{2}[1+1/2(\rho J)]^{-1}\{(\rho J)+(\rho J)^2[\ln(h/2D) + i\pi/2]\}\cdots , \quad (7.4)$$

where the ellipsis is not needed to evaluate the single integration constant K in Eq. (7.1), and where the factor $[1+1/2(\rho J)]^{-1}$ appears because the same factor appears in the redefinition $h\to h[1+1/2(\rho J)]$. This factor is important; it will generate the $e^{1/2}$ in the crossover ratio πW.

Matching (7.4) to (7.1) is straightforward. The result is

$$K = -2D\,|\rho J/2|^{1/2}\exp\{[1+1/2(\rho J)]/\rho J\} = -2e^{1/2}D\,|\rho J/2|^{1/2}\exp(1/\rho J) , \quad (7.5)$$

where the two lines illustrate the origin of this factor $e^{1/2}$. When K is substituted into Eq. (7.1) and compared with Eq. (7.4), the argument of the exponential is determined by the $O(J)$ term. The $|\rho J|^{1/2}$ is required to cancel with $g^{1/2}$, and the rest of the prefactor matches the cutoff $2D$. The role of K as the energy scale of the problem is now obvious.

To complete the discussion of the weak-coupling limit, it is necessary to determine T_H, the high-field scale temperature corresponding to the weak coupling limit used by Wilson. He obtains the large infrared cutoff susceptibility by determining the energy shift of the conduction-electron states, i.e., the effective exchange interaction for the system; this in the absence of conduction-electron polarization. The relevant, here high-field, second-order integral is therefore

$$I_3=(\rho J)^2\int_{-D}^{0}d\varepsilon'\int_{0}^{D}d\varepsilon(\varepsilon'-\varepsilon-h)^{-1}$$
$$\simeq h(\rho J)^2\ln(-2h/eD) \tag{7.6}$$

with the correct definition namely $2pJ_{\text{eff}}=[\ln(H/T_H)]^{-1}$, and since $h=g\mu_B H\simeq 2H$ in the notation of Andrei *et al.*,[3] this corresponds to a high-field scale:

$$T_H=(D/4)|\rho J|^{1/2}\exp(1/\rho J)\ . \tag{7.7}$$

The high-energy cutoff here differs by a factor of 8 from that which helps determine K.

Wilson uses the discretization of his states as an infrared cutoff in the weak-coupling limit. Such a method leaves the polarization of the conduction electrons unchanged. The above integral I_3 uses an almost identical type of cutoff. It must be emphasized that the crossover ratio is sensitive, to within factors of exactly 2, to the details of how the Zeeman energy is, or is not, included in the ultraviolet cutoff.

VIII. STRONG-COUPLING–LOW-FIELD LIMIT

In the preceding section the formula obtained after the first integration of Eq. (5.11) was matched to the high-field perturbative expression. It is remarkable that this procedure is possible, or stated another way, it is surprising that only one of the two integration constants K can be determined by using the weak-coupling limit as a boundary condition. This reflects the fact that for all values of the second integration constant the formula (7.1) gives the same asymptotic expansion. The second integration constant "a" must be obtained by considering the strong-coupling limit.

Given the first derivative g, Σ is determined via Eq. (7.1), once the first integration constant K is given. It follows directly that the specification of g at $h=0$ is equivalent to giving the integration constant a. To determine g, the following requirement are used.

(i) The self-energy is real on the energy shell for $h=0$. This follows since it is conduction-electron–hole pairs which are the heat bath and eventually take away the energy. The relevant phase space on the energy shell is proportional to h, so what is a many-body width associated with the impurity must go to zero in this limit.

(ii) Time-reversal symmetry implies the self-energy cannot contain a linear term in h.

Together (i) and (ii) imply, for small fields, that the self-energy be of the following functional form:

$$\Delta(1+h^2/\Delta^2)+\text{const}\times(ih+\cdots)\ . \tag{8.1}$$

To understand (ii) consider, in general terms, the field dependence of the transverse susceptibility $\langle T[S^+(t)S^-(0)]\rangle$. Since the total Zeeman energy $g\mu_B H(S_z+s_z)$ is a constant of motion, a change in the total spin of unity caused by $S^{\pm}$ changes the energy by $g\mu_B H$. Thus this correlation function has an essential time dependence $e^{ig\mu_B Ht}$. Time-reversal considerations specifically apply to the two-particle self-energy alone. The constraints of time-reversal symmetry then imply that the self-energy must be of the above form. The fact that $\Delta\sim\pi T_0$ is the relevant energy scale will be confirmed later. [There is one alternative. If Σ were zero for $h=0$, then, since this is the transition energy between the two levels associated with the impurity, the corresponding ground state would be doubly degenerate. In fact, this possibility corresponds to the fixed point for the ferromagnetic problem. This is easy to see since from $\Sigma=0$ it follows from Eq. (5.11) that $g=d\Sigma/dh$ is also zero in the $h\to 0$ limit, i.e., the effective coupling constant is zero and the moment decouples itself from the conduction electron sea.]

These analytic properties of the self-energy dictate that

$$\text{Re}\left[\frac{d\Sigma}{dh}\right]=\text{Re}(g)=0 \tag{8.2}$$

for $h=0$.

By particle-hole symmetry the real part of Σ must be odd. Corresponding to a causal function, the imaginary part of the self-energy should also be odd, in which case it turns out to be an analytic function of h.

The value which satisfies the above criterion is unique. For Σ to be real implies $\frac{1}{2}(1/g+\ln g)$ be real plus a possible multiple of $i\pi$. Trivially, $1/g=-i(\pi/2)$ is the only value, less than $i\pi$, for which this is true. While, because of the spectral sum rule, $\text{Im}(I^{\pm})\leq i\pi$. Substitution into Eq. (6.6) gives

$$\Sigma=-4\pi T_0+(2i/\pi)h+\cdots\ , \tag{8.3}$$

where the strong-coupling scale $4\pi T_0$ is given by

$$4\pi T_0=(e\pi)^{1/2}|\rho J|^{1/2}D\exp(-1/|\rho J|)\ , \tag{8.4}$$

which with

$$W'=T_H/T_0 \tag{8.5}$$

is the exact result for the crossover ratio W', although of course it is still necessary to relate πT_0 to the susceptibility.

It is possible to restate the requirements (i) and (ii) in fixed-point language. In general, the scaling Eq. (5.11) is a second-order nonlinear differential equation for a complex self-energy Σ. Writing a separate equation for the real and imaginary parts would result in two such coupled second-order equations. In turn these two equations can be reduced to four first-order equations. Hence there are four conditions $dx_i/dh=0$ required to define a fixed

point, where the x_i are suitable variables in these four differential equations. However, matching the solution to the weak-coupling expansion fixes one complex integration constant, reducing it to a problem in two variables. Because the total magnetization is a constant of motion, a finite magnetic field introduces an essential time dependence to the problem. The limit $h \to 0$ corresponds to a time scale $t \to \infty$. In the long-time, low-energy limit relaxation must cease, leading to requirement (i): $\mathrm{Im}[\Sigma(h=0)]=0$. This reduces the problem to a single first-order equation for $\mathrm{Re}(\Sigma)$, the physical requirement that Σ have a well-defined value in the long-time limit might be interpreted as requiring $\mathrm{Re}(d\Sigma/dh)=0$ for $h=0$.

What has been shown through this study of the two-particle self-energy for the transverse susceptibility is that there is a finite threshold, of order $4\pi T_0$, for excitations of the *impurity* at zero temperature. In Secs. IX and X interest will be in the low-energy spectral density of either the single-particle impurity propagators, in connection with the calculation of occupation factors, or in the low-lying ($\varepsilon < 4\pi T_0$) conduction-electron excitations. The same sequence of diagrams, which contribute to the effective longitudinal vertices, are still identified; however, now, because of this finite energy for excitations which acts as a cutoff, the relevant diagrams have no imaginary parts. To show this formally the calculation will be performed by taking the thermodynamic limit in the nonstandard fashion described in Sec. III; however, this is really unnecessary after it is realized that there is, in fact, such a natural infrared cutoff.

The point of interest in connection with fixed points is that now the relevant solutions of Eq. (5.11) for Σ will be real. In this case the above physical argument cannot be used. In fact, it follows directly from the basic scaling Eq. (5.11) that if $d\Sigma/dh=0$ for $h=0$ then $\Sigma=0$ and, as mentioned earlier, this corresponds to the ferromagnetic fixed point. For the antiferromagnetic case this possibility is excluded. It is useful to examine the fixed and singular properties of the scaling equations itself since these reflect the possible analytic behavior of the different solutions and certain possibilities for the limit $h \to 0$. At face value the scaling equation $dg/dy=2g^2/(1-g)$ has the ferromagnetic fixed point at $g=0$ and singular points at $g=1$ and ∞.

However, except in the weak-coupling limit, this is not an autonomous equation in the scaling parameter h. As noted at the end of Sec. VI, Eq. (5.11) *is* autonomous when written in terms of Z, and so $dZ/dh=0$, or $g=1$ for $h=0$ is a fixed point. In the strong-coupling limit $dg/dy=g^2/(1-g)$ should be considered as an equation for $y(g)$, for which the value $g=1$ gives minimum. This is also a minimum of $Z(g)$. On the other hand, Eq. (6.10) shows g to be a function of h dependent upon the second integration constant a. If a is chosen such that $1/h \to \infty$ implies $g \to 1$, then it follows that $Z(h)$ will approach the fixed point in this limit. [This reflects the asymptotic behavior of a class of solutions of the scaling equations. Since $Z=\Sigma-h$, such solutions $\Sigma(h)$ approach a line of slope unity independent of the first integration constant and Kondo scale K.]

The above few paragraphs on fixed points will not be used directly in the development which follows. They are included only to support the direct development.

It will be useful in later sections to have, in general terms, some knowledge about the two-particle self-energy for the longitudinal susceptibility and other two-particle propagators with antiparallel pairs of impurity lines with the same spin labels.

It is important to realize that such longitudinal propagators have, in general, two branches. This is best illustrated by the two limiting cases when the given propagator couples to only one such branch.

First, let us discuss the simplest case; this corresponds to the propagator:

$$\sum_{\sigma,\sigma'} \langle T_\tau[n_{d\sigma}(\tau) n_{d\sigma'}(0)] \rangle \ , \tag{8.6}$$

i.e., the external vertex is, or effectively is, spin independent. For this case the single-particle self-energies cancel exactly against the vertex corrections. This follows trivially since $n_{d\uparrow}+n_{d\downarrow}=1$ is a constant of motion. This result implies the dressing of the impurity lines cancel exactly for any problem in which all the vertices are spin independent.

The second simple case is for the transverse susceptibility itself, which is proportional to

$$\sum_{\sigma,\sigma'} \sigma\sigma' \langle T_\tau[n_{d\sigma}(\tau) n_{d\sigma'}(0)] \rangle \ . \tag{8.7}$$

Now the external vertex changes sign with spin values. In this case the longitudinal self-energies still cancel with vertex corrections while the vertex corrections double the transverse self-energies. For $h=0$, by symmetry, the frequency dependence of the two-particle self-energy for the longitudinal and transverse susceptibilities must be identical. It follows that approaching $\varepsilon=0$ from positive or negative energy results in an odd self-energy of order $4\pi T_0$. This is important since this form of self-energy generates an infrared cutoff when the conduction-electron "self-energy" is evaluated.

When the external vertices have neither of these simple symmetries a longitudinal propagator involves a sum of the two branches associated with the above two special propagators.

IX. OCCUPATION NUMBERS AND KINK SELF-ENERGIES

So far what has been calculated is the energy of the pole of the transverse susceptibility as a function of the magnetic field. While, as was pointed out in the Introduction, this quantity does have a direct interpretation in terms of the effective longitudinal interaction, it is not directly the object of interest. To calculate the susceptibility it is necessary to calculate the occupation numbers for the impurity. What will be done in this section amounts to a

calculation of the energy of the individual impurity levels. The difference in the energy of these levels is directly related to the pole of the susceptibility when the latter has a small or no imaginary part, i.e., in either the extreme weak- and strong-coupling limits. The result of the preceding section for $4\pi T_0$ will be used to determine the separation of the impurity levels in the strong-coupling limit. The fact that this energy, $4\pi T_0$, is the minimum energy for an excitation of the impurity in this limit implies that the impurity self-energy must be real for energies near the pole corresponding to the ground state, i.e., for deviations in the energy $\Delta E < 4\pi T_0$. Similarly, the conduction-electron "self-energy" will also be real for states which lie within $4\pi T_0$ of the Fermi surface. As would be expected, it is found that the same scaling equation describes the effective vertices in this part of the calculation. However, now, in principle at least, physical quantities of interest will have expansions in terms of these vertices and most importantly the relevant solutions of the scaling equation will be real.

It can be readily appreciated that these real, low-energy effective vertices cannot be smoothly connected to perturbation theory. Clearly they will be singular at an energy of order $4\pi T_0$ when they acquire an imaginary part. Two strong-coupling boundary conditions are therefore required to integrate the scaling equation. One is the energy scale $4\pi T_0$ mentioned above and the other is again obtained by time-reversal arguments.

As was pointed out earlier, the self-energy of the d-electron propagators is not unique. In fact, as a function of frequency (real or complex) these propagators have no physical interpretation. Some of their unusual properties should become more evident from the discussion in this section. However, the d-electron propagators summed over the complex frequency ω_n *do* have such physical interpretation. These give the occupation numbers for the up and down levels. A systematic method is developed in this section, again using repeated partial fraction expansions, for evaluating these occupation numbers.

There is a special problem associated with evaluating occupation numbers using the Abrikosov representation, this because of the single-loop rule. The usual result, that the vacuum polarization diagrams cancel against the partition function in the denominator of a single-particle propagator, does not hold. The partition function must be evaluated separately. Fortunately, the Abrikosov method, because of this defect, has a special, simple rule[6] for the evaluation of the partition function Z (Z should not be confused with the effective cutoff defined in Sec. IV). It is observed, by construction, that the net occupation of the d levels is unity, i.e.,

$$n_{d\uparrow}+n_{d\downarrow}=1 \ . \tag{9.1}$$

However, the individual occupation numbers are not just the sum of the relevant propagator over ω_n, but rather this sum divided explicitly by the partition function, i.e.,

$$Z/Z_0=\sum_{\omega_n}[D_\uparrow(i\omega_n)+D_\downarrow(i\omega_n)] \ , \tag{9.2}$$

where Z_0 is the unperturbed partition function for the conduction electrons. (In principle, Z_0 is the partition function for the full unperturbed Hamiltonian in the Abrikosov representation. In the limit that $\lambda\rightarrow\infty$ only the d-electron vacuum is occupied. It follows that the relevant partition function is the unperturbed conduction-electron quantity).

The occupation numbers are

$$n_{d\sigma}=\sum_{\omega_n}[D_\sigma(i\omega_n)/Z] \ . \tag{9.3}$$

The sums involving $D_\sigma(i\omega_n)$ are tricky. Conventional wisdom dictates that by analytic continuation this should be converted to the form

$$e^{-\beta\lambda}\int d\varepsilon\, e^{-\beta\varepsilon}\mathrm{Im}[D_\omega(\varepsilon)] \ . \tag{9.4}$$

This involves the simplification of the Fermi function $f(\varepsilon+\lambda)=\exp[-\beta(\varepsilon+\lambda)]$ which is valid in the limit $\lambda\rightarrow\infty$. Strictly speaking this formula remains valid; however, it is misleading because there are contributions to the integral where $\mathrm{Im}[D(\varepsilon)]$ is essentially zero. Imagine that $\mathrm{Im}(D)$ is in fact strictly zero for values for ε less than some value ε_0. The significant contribution, in the zero-temperature limit considered here, comes from ε values infinitesimally above ε_0, this because of the extremely rapid decrease of the function $\exp(-\beta\varepsilon)$ with increasing ε. However, in reality $\mathrm{Im}(D)$ has an exponentially small tail for $\varepsilon<\varepsilon_0$, i.e., $\mathrm{Im}(D)\sim\mathrm{const}\times\exp[\beta(\varepsilon-\varepsilon_0)]$. When multiplied by $\exp(-\beta\varepsilon)$ such a contribution is of the same magnitude as that from the "finite" part of $\mathrm{Im}(D)$. It is seen that the zero-temperature limit must be taken very carefully.

This contribution to the occupation numbers which comes from regions where the spectral density is exponentially small in the limit $T\rightarrow 0$ will be called an "admixture" term.

Instead of Eq. (9.4), what works well are the kink methods used in Sec. III. As in earlier sections the method will be illustrated by example. Here it is used to evaluate the occupation numbers so each diagram for the d propagator is implicitly summed over the external frequency ω_n. This allows the internal and external sums to be interchanged, if desired. The general procedure is to repeatedly make partial fraction expansions until either a simple pole is isolated or the result obtained to a given point can be resummed by transferring something times the full propagator back to the left-hand side of the equation.

Again consider the propagator evaluated with just the bare $O(J^2)$ transverse self-energy as implied by the Dyson equation illustrated in Fig. 5. The second and third, previously omitted contribution, in Fig. 6 can be redrawn as in the second line without altering the value. When a second expansion is made between the parts connected by the arrow labeled 2 the result is as shown in the next line. Of the resulting terms the second on the right-hand side involves a frequency sum only on the full propagator. The series can be resummed by transferring this term the left-hand side of the equation. The prefactor to the transferred term is

$$(J/N)^2 \sum_{k,k'} n_k(1-n_{k'})/[h-(\varepsilon_{k'}-\varepsilon_k)]^2 , \tag{9.5}$$

which is just the frequency derivative, $\partial\Sigma/\partial\varepsilon$, of the self-energy with a specific argument $h/2+\lambda$.

Connection with a familiar result is easily made if all but the first and last of the remaining terms are dropped. There is a geometric series, the sum of which is

$$Z^{-1}\left[1-\frac{\partial\Sigma}{\partial\varepsilon}\right]^{-1}[i\omega_n-(h/2+\Sigma_\uparrow+\lambda)]^{-1} = \left[1-\frac{\partial\Sigma}{\partial\varepsilon}\right]^{-1}\exp[-\beta(h/2+\Sigma_\uparrow+\lambda)]/Z , \tag{9.6}$$

remembering there is an implicit sum over ω_n in the first line. The result reflects the usual corrections to the strength, or equivalently to the "charge," and energy of the d-propagator pole. The advantage of the present derivation of this result is that there are explicit expressions corresponding to the remaining diagrams for the contributions usually omitted in this type of approximation.

The terms omitted in the above are not negligible. Consider the $O(J^2)$ term, the third, in line 3 of Fig. 6. Performing the sum over the remaining, ω_n-dependent, central part gives a contribution of the form

$$-(J/N)^2 \sum_{k,k'} \{(1-n_k)n_{k'}/[h-(\varepsilon_{k'}-\varepsilon_k)]^2\} \times\exp[-\beta(\lambda-h/2)]/Z , \tag{9.7}$$

which again involves what at least looks like the derivative of a self-energy. This is multiplied by $\exp[-\beta(\lambda-h/2)]$, the thermal factor for a down spin, because the d propagator within the self-energy is of opposite spin. Notice also the change in the Fermi functions relative to the starting self-energy and that the expression involves the unperturbed expression $\exp[-\beta(\lambda-h/2)]$ because the self-energy is bare. This change in the Fermi functions show that (9.7) is the "admixture" contribution referred to earlier.

A little reflection leads to the generalization of the above results to higher order and including dressed self-energies. There are only three types of terms: (a) kinked self-energies, both direct and overlapping; (b) contributions of the "charge" type; and (c) admixture terms. Both (b) and (c) are proportional to the frequency derivative of some self-energy. In general, the single-particle self-energy will have several denominators either because it is of higher order than second and/or has dressings on the internal d line.

For such higher-order diagrams, one again begins with a partial fraction expansion, the equivalent of 1 in Fig. 5, between the first bare line in the full propagator and the denominators of the self-energy, which corresponds to that part of its diagram to the extreme right. This produces the first kink. There are two types of terms. First, ones which still involve the last denominator of the self-energy, the equivalent of the second and third terms in Fig. 6, and one term proportional to the external d line involved in this first partial fraction expansion, i.e., the equivalent of the last term on the first line of Fig. 6. The difference here is that this last term is not yet a kink self-energy because there still remain horizontal parts of the original single-particle self-energy. One therefore continues the equivalent of expansion 1 until all parts of the self-energy are vertical. With each such expansion new contributions are generated which are grouped with the second and third terms of Fig. 6 and which can all be rewritten as between lines one and two of this figure. The partial fraction expansion 2 then generates terms that are the equivalent of the second term in the third line of Fig. 6 which modifies the "charge" and is used to resum the series. There are many of the third admixture contributions which involve the poles of the single-particle self-energy and which will be taken up again below. Lastly, there are terms not illustrated in Fig. 6 which are dressing of the vertical (external) line, i.e., the down pointing, or right-hand vertical, part of the kink. This is illustrated in Fig. 7. The net result is an additional internal dressings of the kink self-energy. In fact, the internal dressing is simply the two-particle self-energy associated with the antiparallel impurity lines involved in the kink.

To understand the general nature of the admixture contribution consider reordering the sums in the evaluation of n_d in such a way that the diagram would be drawn as shown in Fig. 23. It is implied that the sum over the frequency which passes though the d line that was at the interior of the self-energy is performed last. The large cross indicates the equivalent of an external vertex but with an associated frequency which is zero. Isolating the contribution from this last d line using the kink methods produces an admixture term which involves the frequency derivative of the self-energy times the exact occupation number both for what was the interior d line of the original self-energy diagram. Again it is found that the self-energies which enter the denominator of this self-energy derivative are the relevant two-particle self-energies.

Using this kink formalism to perform repeated partial fraction expansions for particular examples it has always proved possible to classify each contribution as belonging to one of the three classes of contributions discussed

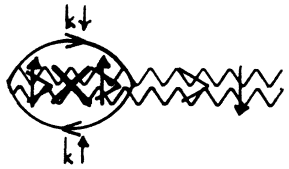

FIG. 23. When the frequency sums involved in evaluating the occupation numbers are recordered, the transverse $O(J^2)$ contribution to Dyson's equation, Fig. 5, can be redrawn as shown in this figure. Here all d propagators are assumed dressed and the point of redrawing the diagram in this fashion is to imply the frequency sum on the d propagator to the right is done last. Clearly, as drawn, this is the derivative of the down-spin self-energy times the full down-spin propagator. This result is used in the text.

above. Recall though that there *are* more complicated "overlapping" kink diagrams such as that shown in Fig. 8. As discussed in connection with the two-particle self-energy, these play a role identical to that of vertex corrections. The conclusion for an isotropic interaction is again that these corrections cancel. The details of this particular cancellation will not be given since it is related to that demonstrated in the Appendix.

It is implied that the general result for the occupation number can be written as

$$n_{d\sigma}=n_{d\sigma}^{E}+\left[\frac{\partial\Sigma_{\sigma}}{\partial\varepsilon}\right]n_{d\sigma}-\left[\frac{\partial\Sigma_{-\sigma}}{\partial\varepsilon}\right]n_{d-\sigma}\ , \tag{9.8}$$

where $n_{d\sigma}^{E}$ is the elementary occupation number:

$$n_{d\sigma}^{E}=\exp[-\beta(\sigma h/2+\lambda+\Sigma_{\sigma})]/Z\ , \tag{9.9}$$

where, although the formula is more general, here this quantity is unity or zero because the temperature is taken as zero. The n_{d}^{E} which is unity corresponds to the ground state. Note that the "self-energy" Σ_{σ} in the last two expressions is not the single-electron self-energy but rather the kink inclusion (or kink "self-energy") discussed above. In particular, it contains the relevant two-particle self-energy in the denominator and there are overlapping contributions. The result (9.8) takes advantage of a cancellation which occurs between the two types of derivative terms, i.e., the charge and admixture terms, when the internal d line of a self-energy is the same as the external lines. As a result Σ_{σ} contains only the spin-dependent part of the kink "self-energy." The spin-independent term in (9.9) is absorbed into λ. Again it is emphasized that the last term in Eq. (9.8), involving $n_{d-\sigma}$, is an admixture contribution corresponding to the troublesome exponential tails. Involved in the diagram are intermediate states in which the conduction-electron contribution to the energy is negative, e.g., in a simple diagram such as Fig. 3(a) the sum $\varepsilon_{k\uparrow}-\varepsilon_{k'\downarrow}<0$ is opposite in sign to that implied by the thermal functions $(1-n_{k})$ and $n_{k'}$ associated with the self-energy. This is important when the relevant branch of the internal $d-\sigma$ self-energy is to be determined.

The final question of technique is the treatment of the imaginary parts of the kink self-energies. It is desirable to actually force the conduction-electron self-energy to be real. As was shown in connection with simple potential scattering in Sec. III, if the limits $s\to 0$ and the thermodynamic limit $1/N\to 0$ are taken in that order, then it is possible to define a non-Dysonian "self-energy" for the conduction electrons, which unlike the usual prescription, gives directly the quasiparticle energy. In this section and the remaining sections of this paper this trick will be used in order to directly obtain the ground-state properties. Of course, physical results should not depend upon the use of this or the more usual method of taking the thermodynamic limit; this less standard method simply makes the task much easier. In fact, this trick is really unnecessary since, as discussed at the beginning of this section, there is a natural infrared cutoff $4\pi T_{0}$ in the problem which removes the need for this ruse.

All that remains is to identify and evaluate the self-consistent leading parquet approximation for the kink itudinal diagrams as skeletons. The beginning of this longitudinal series is shown in Fig. 24. Ignoring band-edge effects and without an infrared cutoff all but the $O(J)$ kink self-energies are zero. However, with a cutoff C the $O(J^{2})$ contribution is proportional to $C(\rho J)^{2}\ln(C/D)$. The $\ln(C/D)$ terms in $O(J^{3})$, and other odd orders, cancel so that with the self-consistent leading parquet approximation there is no spin dependence (the cutoff C to be spin independent) to terms other than $O(J)$. The next step is to consider the $O(J^{2})$ renormalization $L\to TT$ of the longitudinal vertices. This is more involved than it was for the two-particle self-energies. It is necessary to extract the field dependence of each diagram. It is easy to show that all three TTL, TLT, and LTT diagrams are required to obtain the leading logarithmic term proportional to the field h. In fact, for the kink self-energies the contribution $TTL=LTT=\frac{1}{2}(TLT)$ so that the three terms are equal to $2(TLT)$. On the other hand, as discussed in the Introduction, the existence of time-reversal conjugate diagrams shows that when the replacement $L\to TT$ is made more than twice there is no contribution proportional to h. Taken with the above for the skeleton longitudinal diagrams this implies that there is no contribution to leading parquet approximation from such diagrams. These diagrams contribute a field and spin-independent kink self-energy which might be absorbed into the projection energy λ. The only relevant diagrams correspond to repeated replacements $T\to TL$ so that such diagrams never have more than two T vertices. The fact that these diagrams are sufficient can be deduced inductively from the arithmetic for $O(J^{3})$. The result is a total contribution equal to $(2)^{n}TLLL\cdots LLLT$, where n is the number of L vertices. Finally, as was the case for the two-particle self-energy, and for the same reason, the relevant dressing of the internal lines is longitudinal. What is obtained in this way is that part of kink "self-energies" for the single-particle impurity propagators which is dependent upon the impurity spin. These will be denoted $\Sigma_{\sigma},\sigma=\uparrow$ or $\downarrow$. In the asymptotic, large-field limit the spin-dependent part of these "self-energies" are equal and opposite. However, in the strong-coupling limit this is not the case except for exactly $h=0$. This will be investigated below.

Taking the derivatives with respect to the field gives the *same* universal scaling equation for twice $-\Sigma_{\uparrow}$ or $\Sigma_{\downarrow}$ as for the two-particle self-energy. Although the scaling equation is the same the useful solution of (5.11) for the

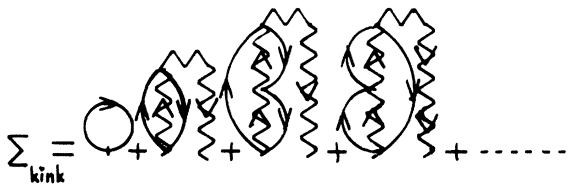

FIG. 24. Beginning of the longitudinal series drawn as kink "self-energies." Ignoring ultraviolet, i.e., band-edge and infrared cutoff effects, all but the $O(J)$ contribution can be ignored. The infrared cutoff generates field-independent terms which can be absorbed into the projection energy λ. Band-edge effects are negligible.

kink self-energies is not that given by Eq. (8.3). Rather, as discussed above, a real solution is required. However, the value of $\Sigma=-4\pi T_0$ for $h=0$ can be used as a boundary condition for this new solution. Physically, the complex two-particle and real kink self-energies must agree when the imaginary part of the former is zero, since then both give the exact energy for the transition $S_z=-\frac{1}{2}$ to $S_z=\frac{1}{2}$. More formally, it is noted that $-2\Sigma_\uparrow$, $2\Sigma_\downarrow$, and Σ are given by identical expressions in terms of impurity two-particle self-energy, i.e., Σ itself. All three therefore correspond to the transition energy $S_z=-\frac{1}{2}$ to $\frac{1}{2}$ at the one common point $h=0$. However, each can, and does, have a different behavior for finite h. Finite h moves Σ into a region where it is complex, while $-2\Sigma_\uparrow$ and $2\Sigma_\downarrow$ belong to manifolds with different total values of the spin, and for this reason have a different field dependence as will be shown below. Hence this identification of the $h=0$ values of these "self-energies" gives only one boundary condition on a second-order equation and still leaves the derivative of the real kink self-energies to be determined.

The second boundary condition follows if the ground state is to reflect the requirements of time-reversal symmetry. Because the kink "self-energies" determine the energies which enter the partition function, not only do they correspond to exact energies but the lowest such energy corresponds to the ground state. In turn, since the ground state is not degenerate the leading term in the field must be h^2. The linear in h term in the kink "self-energy" must cancel the explicit Zeeman energy $h/2$. This implies $\partial 2\Sigma/\partial\varepsilon(=g)=-1$, giving the second boundary condition necessary to fix the real solution $-2\Sigma_\uparrow$ for small h and for up spin, corresponding to the ground state. Note, the absence of a term linear in h in the ground-state energy *reflects* an absence of a spontaneous magnetization. For $h=0$, Eq. (5.11) yields $d^2\Sigma/dh^2=-2g^2/\Sigma$, which gives the expansion

$$\Sigma_\uparrow(h)=\tfrac{1}{2}(-4\pi T_0-h+h^2/4\pi T_0+\cdots)\,. \tag{9.10}$$

The spin-dependent part of the down-spin kink "self-energy" has the opposite value $\frac{1}{2}4\pi T_0$ for $h=0$. It is tempting to simply assume again $\partial 2\Sigma/\partial\varepsilon(=g)=-1$. (The derivative with respect to the field, h, and energy now differ in sign.) This turns out to be wrong. Physically the value of g for the down-spin line corresponds to a state with a different value of the total spin and might therefore be expected to be different. This second effective exchange will be denoted g^*.

$$n_{d\uparrow}=1+\tfrac{1}{2}(gn_\downarrow-g^*n_{d\downarrow}) \tag{9.11}$$

or

$$n_{d\uparrow}-n_{d\downarrow}=1+(gn_{d\uparrow}-g^*n_{d\downarrow})\,. \tag{9.12}$$

with $g=1$.

As noted above, the absence of a term linear in h when Eq. (9.10) is added to the Zeeman energy reflects the absence of a finite magnetic moment for $h=0$. If then $n_{d\uparrow}-n_{d\downarrow}$ is to be zero, it must be $g^*=+1$. This gives

$$\Sigma_\downarrow=\tfrac{1}{2}(4\pi T_0-h-h^2/4\pi T_0+\cdots)\,. \tag{9.13}$$

It must also be recognized that each of Eqs. (9.10) and (9.13) have two branches. As was pointed out in Sec. V in connection with Eq. (5.8), the individual expressions for $\Sigma_\uparrow$ and $\Sigma_\downarrow$ are odd. It follows that the first and third terms on the right-hand side, and all terms even in h, change sign with the sign of h or the energy. As was pointed out above, the intermediate-state energy associated with the "exponential tail," i.e., the admixture g^* term in Eqs. (9.11) and (9.12), is negative while (9.13) corresponds to positive values of h. The branch which determines g^* in (9.11) and (9.12) is therefore not the same as that for (9.13).

Finally, substituting the relevant values for the derivatives into Eq. (9.12) for the polarization gives the impurity susceptibility. The derivatives with respect to the energy are equivalent to derivatives with respect to the field h for up spin and $-h$ for down spin. Taking the appropriate branches this gives

$$\frac{d\Sigma_\uparrow}{d\varepsilon}=g=-1+h/4\pi T_0+\cdots \tag{9.14}$$

and

$$\frac{d\Sigma_\downarrow}{d\varepsilon}=g^*=+1-h/4\pi T_0+\cdots\,, \tag{9.15}$$

i.e., to the order displayed, $g^*(h)=-g(h)$. Substituting into Eq. (9.12) yields a susceptibility,

$$\chi=(\mu_B)^2/\pi T_0\,, \tag{9.16}$$

which is the *exact result.* Recall, since the g factor is 2, $h=2H$, ignoring $O(\rho J)$ corrections.

The fact that this is the full impurity susceptibility reflects the compensation theorem. Equation (9.16) is reproduced directly from the quasiparticle energies in the next section. The fact that the compensation theorem is satisfied is also discussed. As a consistency check, it is noted that if the wrong branch of Eq. (9.13) were taken for the evaluation of (9.15) the impurity susceptibility would be zero and the compensation theorem would not be satisfied.

The fact that $g=-g^*=-1$, demonstrates explicitly, within the present formalism, the well-known result that only one electron per scattering channel compensates the impurity. This results from time-reversal considerations once it is determined that the ground state is energetically nondegenerate.

This relationship between the g's is very important for another reason. It is the exact opposite of the perturbation limit when $g^*=g$, and shows that the effective impurity-conduction-electron interaction is purely potential in the strong-coupling limit, i.e., it is of the form

$$-t(\varepsilon)(n_{d\uparrow}+n_{d\downarrow})\,, \tag{9.17}$$

where t is some parameter. These conclusions about the nature of the strong-coupling fixed point are consistent with those of Wilson. It will be used as a check in the next section.

It is seen that then the requirement $g=-1$ for the up-spin ground state corresponds to the down-spin excited state $g=+1$, i.e., the value corresponding to the fixed

point of the general scaling equation. Since the one limiting value implies the other, the value $g=-1$ is also seen to correspond indirectly to one of the significant limiting points of the scaling equation.

X. CONDUCTION-ELECTRON PROPAGATORS

The last step in the present development is the calculation of conduction-electron quantities for states close to the Fermi surface and in the strong-coupling limit. This will permit the (re)calculation of the susceptibility, the specific heat, and the resistivity.

Because of the single-loop rule, for a single impurity, there is no self-energy for the conduction electrons in the Dysonian sense. It should not be surprising that there is no such self-energy part; after all, as was discussed in Sec. III, there is not even such a self-energy for the single-impurity potential scattering problem. However, there is a well-defined t matrix and/or reaction matrix and the quasiparticle energies can be determined from its poles. This can be used to define an effective "self-energy." In order to directly obtain real energy corrections the limits $s\to 0$ and $2D/N\to 0$ will be taken in this inverted order and lead to a reaction matrix formalism.

It is possible to define a self-energy for a system with a finite concentration of impurities. The finite concentration problem is also the most direct way of evaluating the resistivity. These alternative methods will be discussed towards the end of this section. In this case the regularization of the model is of a more usual form.

The conduction-electron scattering matrix is the sum of two three-particle propagators. One such propagator corresponds to the longitudinal self-energy and the other to the transverse or spin-flip self-energy, both are illustrated in Fig. 25. However, whichever self-energy is considered the intermediate states can individually be classified as either longitudinal or transverse, depending upon whether they contain antiparallel lines of the same or net different spin.

Consider an nth-order contribution to the scattering matrix; it contains n local moment lines but only one Abrikosov projection factor $e^{\beta\lambda}$. As noted earlier, the local moment lines are all assigned positive complex frequencies in order that the contribution from the pole of any impurity propagator is proportional to $e^{-\beta\lambda}$. Because there is only one projection factor there can only be one impurity propagator per diagram which contributes. The corresponding thermal function is either $n_{d\uparrow}$ or $n_{d\downarrow}$, which serves to classify contributions into one of two classes. Clearly no repeated part of a diagram can contain an impurity thermal function. Such repeated parts of the scattering matrix lead to the energy correction or "self-energy" for the quasiparticle poles. Because there is no thermal function in the "self-energy" the relevant diagrams can again be evaluated by essentially the same rules of thumb used earlier. The only significant difference which stems from the (odd) three-particle nature of the propagator is the absence of the factor $(-1)^{n_e}$ associated with n_e, the number of electron lines which lie on the right-to-left—directed impurity line.

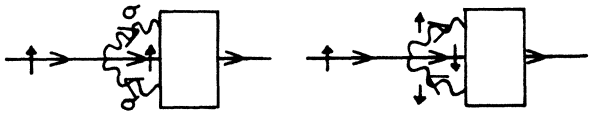

FIG. 25. Conduction-electron self-energy can be considered as being the sum of two three-particle propagators as illustrated here. Each such contribution has a prefactor of a d-electron occupation number, but does not involve repeated factors which contain such occupation numbers.

When evaluating conduction-electron quantities, the Abrikosov representation of Sec. II, Eq. (2.4), which includes the potential scattering in the longitudinal exchange vertices will *not* be used. Rather, it is somewhat easier to use the standard version of the representation and account for the potential scattering by standard techniques as, for example, illustrated by the diagrams in Fig. 4. However, the potential scattering is irrelevant to the strong-coupling limit and so, in practice, will be ignored.

To better understand the nature of the counting problem it is useful to consider the simple-impurity scattering problem in its own right using the Abrikosov representation. The combination $n_{d\uparrow}+n_{\downarrow}=1$ is inserted in the potential scattering term $v\sum_{k,k'}a_k^\dagger a_{k'}$ to give

$$v\sum_{k,k'\sigma,\sigma'}a_{k\sigma}^\dagger a_{k'\sigma}d_{\sigma'}^\dagger d_{\sigma'}\ . \tag{10.1}$$

The point of the exercise is to compare the Abrikosov diagrams in Fig. 26 with the regular impurity scattering diagrams shown in the same figure. The corresponding is indicated. The related diagrams have the same value, and therefore without needing to evaluate them it is clear that the remaining diagrams cancel.

The longitudinal diagrams for the present problem have an identical structure, the only difference is the sign of the vertices change when the spin labels are changed. This does not materially change things and only the same subset of diagrams, as for simple-impurity scattering, are required. Notice, however, because of this spin dependence of the vertices, the internal impurity lines will carry a noncanceling dressing corresponding to the case discussed in Sec. VIII in relation to the propagator (8.6). Notice also the two diagrams [Figs. 26(b) and 26(c), which differ in that one conduction-electron line has been transferred from the right to the left directed impurity line], add to give a contribution which is not logarithmic divergent near the Fermi surface, i.e., the logarithmic divergent parts of the two individual diagrams cancel. In contrast, if an extra minus sign were needed when the line is transferred the logarithmic contributions would add. On the other hand, because of the different sign for the longitudinal vertex *inside* a transverse diagram the logarithmic parts of the two diagrams in Fig. 27 *do* add. [Incidentally, Coleman's vertex correction generates Fig. 26(b) but not Fig. 26(c), and therefore the cancellation of the logarithmic part does not occur without vertex corrections.]

The totality of relevant diagrams are counted, as in earlier sections, by taking the important longitudinal diagrams as skeletons and dressing their vertices. The elementary $O(J)$ longitudinal vertex has an $O(J^2)$ dressing shown in Fig. 28. The leading logarithmic series is then

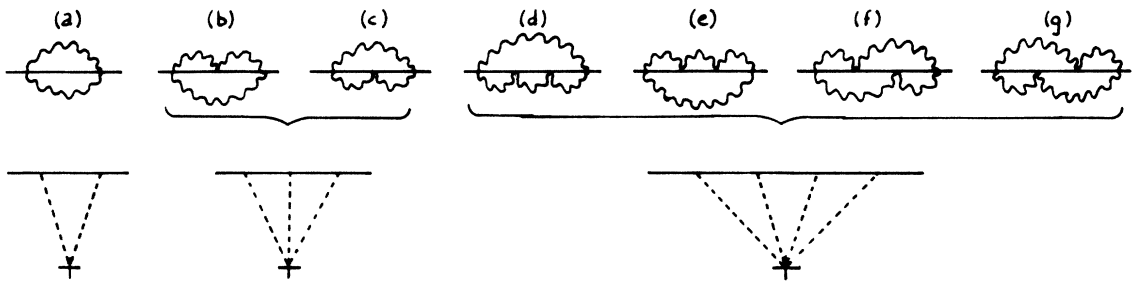

FIG. 26. Correspondence between potential scattering diagrams in the Abrikosov representation and those in the standard multiple-scattering formalism. While, in general, there are more diagrams in each order of perturbation theory with the former method, the sum of the diagrams shown in equal to the diagrams of the standard formalism shown below. Other diagrams in the fourth order and beyond cancel.

generated by including longitudinal vertices *between* the transverse ones, in all possible ways. The four relevant time orderings which increase the order of a diagram by one, for the first of the illustrated vertices, are shown in Fig. 29. Dressing a vertex with longitudinal vertices which lie to the exterior of the transverse vertices corresponds to some dressing of another skeleton and must not be included.

This prescription is in agreement with the usual one: $T \rightarrow TL$ plus LT and $L \rightarrow TT$ for generating the leading logarithmic series. Here, e.g., $T \rightarrow TL$ means that the next higher order is obtained by replacing a T vertex with a T vertex with a TL combination connected by an extra electron line. However, again it might seem surprising that this is used to generate only the simple combination of vertices $TLL \cdots LLT$ in all orders.

The effective "self-energy" $\sigma_\sigma(\varepsilon)$ which corrects the energy of a quasiparticle with spin σ corresponds to the multiple scattering diagrams shown in Fig. 30. First, corresponding to bare longitudinal vertices, to $O(J)$, $\sigma=(J/2)S_z$ for the up-spin quasiparticle illustrated in the figures. The $O(J^2)$ parts are illustrated in Figs. 30(c)—30(f). This purely longitudinal contribution is certainly not logarithmic divergent; however, it must be recalled that the scheme which generates the real "self-energy" involves retaining a finite infrared cutoff $C \sim 2D/N$, which for the purely potential scattering problem of Sec. III leads to the $\pi \tan \pi x$ term in addition to the usual principle part. This requires further examination.

The difference between the present and potential scattering problem is the presence of a natural infrared cutoff of order $4\pi T_0$. Because the longitudinal vertex changes sign with spin label, the relevant dressing corresponds to the propagator (8.6) of Sec. VIII and has a value $\pm 4\pi T_0$ for small positive or negative energies. This finite value for the self-energy provides an infrared cutoff. Because of this cutoff the $\pi \tan \pi x$ term is absent, leaving only the negligible principle part. Further discussion of this important point is to be found in Sec. XI.

The self-consistent parquet approximation for the energy corresponding to the poles of the scattering matrix is therefore obtained by simply summing the TT, TLT, $TLLT, \ldots, TL \cdots LT$ series referred to above. Finally, since the interior of σ is transverse the impurity lines should be dressed with the longitudinal self-energies for the same reason as the longitudinal self-energy was included, to make the calculation self-consistent, in each of the earlier parts of the calculation. As would be expected, since this is the effective interaction vertex, the result for the effective "self-energy" (i.e., the energy correction to the poles) within the self-consistent parquet approximation is given in terms of the quantity g introduced earlier:

$$\sigma_\sigma(\varepsilon) = -(\sigma S_z/N\rho) g(\varepsilon - \sigma h) . \tag{10.2}$$

The dependence upon the field has been explicitly included in the argument.

The fact that $\sigma(x)$ is given in terms of $g(x)$ still leaves a problem, since in fact there are two g's, the one denoted simply g and g^*, and two branches for each g. The relevant "g" is fixed by comparison with the results of the preceding section.

The diagrams shown in Fig. 29 are the beginning of those for the "self-energy" of the up-spin quasiparticles. A comparison of the effective vertices involved with those

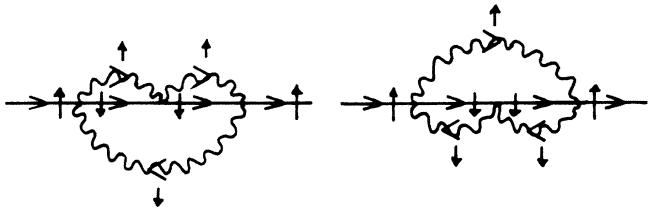

FIG. 27. While the logarithmic parts of Figs. 26(b) and 26(c) cancel, those of the transverse diagrams shown here add to generate the $O(J^3)$ contribution to the effective longitudinal interaction.

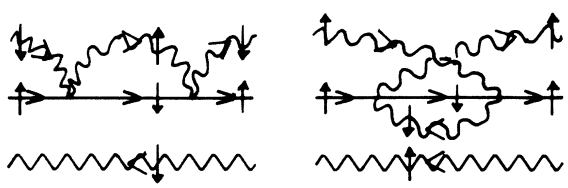

FIG. 28. The two $O(J^2)$ vertices which dress the $O(J)$ vertex to generate the first terms in the logarithmic series.

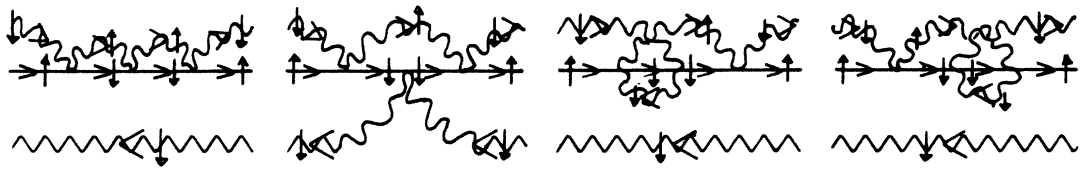

FIG. 29. These diagrams are of third order and generate the next logarithmic order after the digrams Fig. 29. Each diagram in the time ordering shown is of the form $TLLT$. The next order in the $TL\cdots LT$ series is obtained from the previous order in the same way.

in the impurity diagrams shows, for such a quasiparticle below the Fermi surface interacting with an $S_z=\pm\frac{1}{2}$ impurity line, that the effective longitudinal interaction vertex is the same as that denoted g in the preceding section. On the other hand, if the impurity spin sign is changed the relevant vertex involves g^*. The results for the opposite-sign quasiparticles can be determined by the particle-hole-spin symmetry of the Hamiltonian. With this the net self-energy $\sigma_\sigma(\varepsilon)$ is spin independent. Because of this and corresponding to the discussion of the propagator (8.5), the quasiparticle poles are not shifted by the impurity dressing. Again, further discussion of this is to be found in Sec. XI.

With the expansions for $g^*(\varepsilon)$ or $g(\varepsilon)$ obtained in Sec. VIII the various results can be summarized by the following, in the strong limit:

$$\sigma_\sigma(\varepsilon_{k\sigma})=(1/2N\rho)[1-(\varepsilon_{k-\sigma}/2\pi T_0)+\cdots], \tag{10.3}$$

where the value $\varepsilon=\varepsilon_{k\sigma}$ appropriate to the energy shell has been used. This result coincides with Nozières's model,[19] i.e., the quasienergies are

$$\varepsilon_{k\sigma}=\varepsilon^0_{k\sigma}+(1/2N\rho)[1-(\varepsilon_{k-\sigma}/2\pi T_0)+\cdots]. \tag{10.4}$$

The density of states is obtained by differentiation:

$$N_\sigma(\varepsilon)=\frac{dn}{d\varepsilon}=\rho(1+(1/N\rho)[(\varepsilon-\sigma h)/4\pi T_0]+\cdots), \tag{10.5}$$

which is consistent with an Abrikosov-Suhl peak pinned to the opposite-spin Fermi momentum. This density of states corresponds to a susceptibility:

$$\chi=(\mu_B)^2/\pi T_0 \tag{10.6}$$

and a ratio:

$$R=[(\Delta\chi/\chi)/(\Delta C_v/C_v)]=2. \tag{10.7}$$

The susceptibility is double that expected from the density of states at the Fermi surface because the "self-energy" is a function of $\varepsilon_{k-\sigma}$ rather than ε_k, which would not double the susceptibility, or $\varepsilon_{k\sigma}$, which would have the peak pinned to the same spin Fermi surface and would result in there being no contribution to the susceptibility from the change in the density of states.

Finally, this susceptibility corresponds to a crossover ratio:

$$W'=T_H/T_0=(\pi/e)^{1/2}, \tag{10.8}$$

confirming again that the present methods yield exact results.

Because of the potential-like form of the effective interaction in the strong-coupling limit, Eq. (9.17), it is possible to write a simple expression for the exact conduction-electron propagator. Using the same methods as above to sum the series, the two contributions to the scattering matrix simply add in such a way that the result is proportional to $n_{d\uparrow}+n_{d\downarrow}=1$, so the exact propagator near the Fermi surface is

$$G_{k\sigma}(\varepsilon)=\{\varepsilon-[\varepsilon_{k\sigma}+\sigma(\varepsilon-\sigma h)]\}^{-1}, \tag{10.9}$$

the expected simple form for fermonic quasiparticles. [To be more specific, excluded from (10.9) are poles with associated energies which lies $4\pi T_0$ or more away from the Fermi surface.]

Having obtained the relevant exact results for the single-impurity limit it is perhaps interesting to turn to the finite, but small concentration problem using the con-

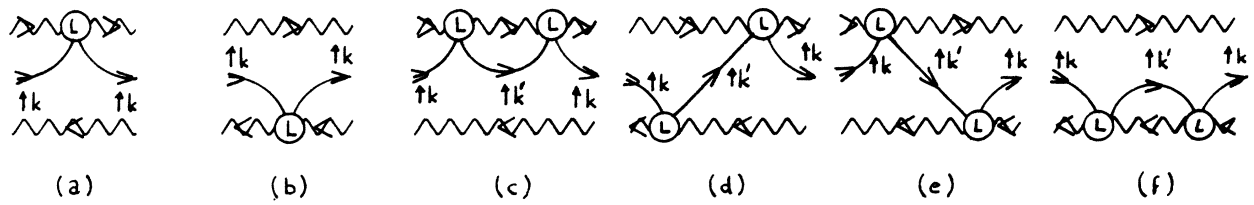

FIG. 30. Dressed longitudinal series. The dressed $O(J)$ contribution (a) generates the leading parquet approximation. Because of the nature of the Kondo problem there is a natural infrared cutoff or order πT_0 which suppresses the size-dependent $\pi\tan\pi x$ term that was generated in the potential scattering problem considered in Sec. III.

ventional method to take the thermodynamic limit. With this it is possible to obtain the resistivity in a direct way. Since the results obtained above are of the form of those for simple potential scattering the relevant formulas can be deduced from a comparison between those derived in Sec. III. In particular, the t matrix which yields the energy shift (10.4) is written down. Combining this with the usual impurity averaging technique[13] gives, for the conduction-electron self-energy,

$$\sigma_\sigma(\varepsilon)=(c\Delta/\pi\rho)/[i\Delta-(\varepsilon-\sigma h)] , \tag{10.10}$$

where the width $\Delta=4T_0$ and c is the concentration. While this result is suggestive of a Lorentzian it does not contain the higher-order term of an expression in ε/Δ. Again there is a Abrikosov-Suhl resonance at the Fermi surface. Also, by construction, the resistivity agrees with that predicted by Eq. (10.4) when the energy shift is interpreted as δ/π, where again δ is the phase shift. Following Nozières,[19] the zero-field conductivity is

$$\sigma_0=\tfrac{1}{3}\pi\rho^2 v_F^2 e^2/(c\sin^2\delta) , \tag{10.11}$$

where for $h=0$, $\delta_0=\pi/2$, i.e., $\sin^2\delta=1$. Using either Eq. (10.4) or (10.10), the phase shift for a finite field is related to the polarization, $m=\rho(\delta_\uparrow-\delta_\downarrow)/\pi$ via, e.g.,

$$\delta_\uparrow=\delta_0-\pi m/2\rho=\delta_0-(\pi\chi/2\mu_B\rho)H .$$

Finally, this section provides a discussion of the compensation theorem. It turns out that if instead of using symmetry one carefully examines the effective vertices involved, then Eq. (10.3) is not strictly correct. The down-spin "self-energy" should involve g rather than g^* with the net effect that the first term in the expansion, Eq. (10.3), should have an opposite sign for this spin direction. This does not alter the quasiparticle energies near the Fermi surface, since the phase shifts $\pm\pi/2$ both move a given level in such a way that it lies midway between two of the original unshifted levels, i.e., odd N levels become even N levels, as in Wilson's work. The fact that the phase shift is opposite *does* imply a net change of polarization of the quasiparticles. This correctly reflects the compensation of the impurity. In the weak-coupling limit, because the field is large the spin is along the direction of the field. Using the same argument that leads to the Friedel sum rule implies opposite phase shifts corresponding to the unitarity limit, i.e., $\delta_\uparrow=-\delta_\downarrow=\pi/2$, if there is to be no net moment localized near the impurity site in the strong limit.

There is, however, no net polarization of the conduction electrons; this reflecting the compensation theorem. To see this the polarization is obtained via the usual formula:

$$m=\tfrac{1}{2}(g\mu_B)\sum_{\omega_m,k}[G_{k\uparrow}(i\omega_n)-G_{k\downarrow}(i\omega_n)] . \tag{10.12}$$

It is necessary to perform the sum over the complex frequency for the exact propagator and this gives different results. Explicitly this is done using the kink methods. Consider the $O(J^2)$ contribution as drawn in Fig. 31(a). This is a vacuum polarization diagram which has been differentiated with respect to one of the conduction-electron energies ε_k. Such a differentiation generates two types of terms. First, the one coming from the differential of the thermal function n_k associated with the energy ε_k. A second set of terms comes from differentiating the denominators which contain this same energy. The former contribution corresponds to the $O(J^2)$ kink self-energy for the quasiparticle, i.e., a term which appears in the exact ε_k. The latter terms can be written as the derivatives of *impurity* kink "self-energies," see Fig. 31(b), essentially in the same way as such terms were obtained in Sec. IX in connection with the d-electron occupation numbers. In fact, the total of these terms are identical, except for a sign, to the similar terms involving derivatives found in that section, i.e., there is an "admixture" term:

$$\tfrac{1}{2}(g\mu_B)(gn_{d\uparrow}-g^*n_{d\downarrow}) .$$

This exactly cancels the conduction-electron polarization and represents a generalization of the perturbation-theory result. [This, of course, ignores the $O(J)$ term which is negligible in the scaling limit.]

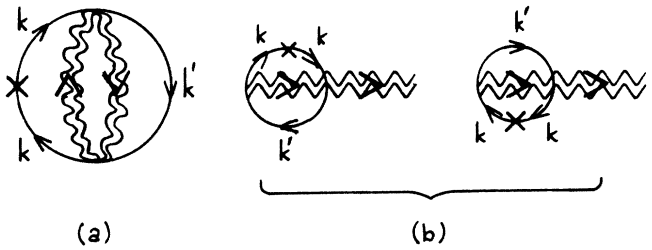

FIG. 31. By reordering the frequency sums, the contribution to the conduction-electron occupation number illustrated in (a) can be cast in either of the forms (b). These alternative forms illustrated there is a contribution proportional to the occupation number of the propagator to the right of these two diagrams times the derivative of the corresponding d-propagator self-energy. The conclusion is related to that associated with Fig. 23, except here the derivative is generated by splitting the conduction electron rather than the d-electron line. This notwithstanding, these "admixture" terms are equal to those in magnitude but opposite in sign, a generalization of the perturbation-theory result.

XI. DISCUSSION AND CONCLUSIONS

In this paper the author has developed a new approach to the construction of a scaling theory for the Kondo problem. The resulting theory leads to exact results for the strong-coupling limit. Rather than treating the effective conduction-electron interaction at the Fermi surface as the fundamental quantity, here attention is focused upon Σ, which is a self-energy for the transverse susceptibility. In the weak-coupling limit this can be viewed upon as the energy required to make a sudden spin flip of the impurity spin. In general, it determines the energy required to excite the impurity from a ground state to an excited state, and in particular, in the strong limit, it corresponds to the energy required to make a transition from the singlet ground to the triplet excited state. The quantity which plays the role of an effective interaction is

$g = d\Sigma/dh$. Here h, the field in energy units, is used to control the cutoff in the logarithmic integrals of the theory.

It is emphasized that the invariant charge g, i.e., the variable in the scaling equation, is not unique and the present choice of such a charge is different from that in the scaling theory of Abrikosov and Migdal.[10] It is argued that there must be an optimal choice of the invariant charge. With such a choice the susceptibility, and other quantities, *in the strong-coupling limit,* are simply related to the charge. Historically, it has not proved possible to obtain *any* results for the strong-coupling limit using the invariant charge chosen by Abrikosov and Migdal.

Also of importance is the fact that the present choice of invariant charge leads to the especially simple scaling equation:

$$\frac{dg}{dh} = g^2/(1-g) . \tag{11.1}$$

This is of closed form and, as a result, is capable of coupling the weak to strong limit.

It is shown that Σ, on the relevant energy shell, is real and finite in the strong-coupling limit when the field $h \to 0$. This value of Σ corresponds to the energy required for the transition marked 1 in Fig. 19. This is the smallest energy which causes a transition to an excited state *of the impurity* and directly implies that the ground state associated with the impurity is nondegenerate in this same limit. In turn it can be readily appreciated, from the requirements of time-reversal symmetry, that this energetic singlet must also correspond to a spin singlet.

In order to calculate the impurity susceptibility one is led to study the single-particle propagators for the Abrikosov fermions associated with the $S_z = \pm\frac{1}{2}$ levels. This introduces two new but related quantities denoted Σ_σ. The $\Sigma_\sigma/2$ are the spin-dependent part of a (kink) "self-energy" for the single-particle propagators. Given the finite energy to the first excited state of the impurity (and zero temperature), the "self-energy(ies)" of interest are real.

For $h = 0$, the difference between the spin-dependent parts of the single-particle (kink) "self-energies" and the value two-particle self-energy, placed on shell, correspond to the same transition energy i.e., again that marked 1 in Fig. 19, and *must* have the same value. This provides one boundary condition for the integration of the scaling equation for Σ_σ. The second boundary condition needed to obtain a solution in the strong limit is again obtained by time-reversal symmetry. It is found that, in fact, the Σ_σ have different expansions which meet at $h = 0$. These are *two* relevant values for $d\Sigma/dh$, one for each of the $S_z = \pm\frac{1}{2}$ propagators. These values are $g = -1$ and $g^* = +1$.

To understand the physical origin of this differentiation between g and g^*, consider the relative orientations of the conduction electron and impurity spins for a given manifold of fixed total z component of the spin, $S_z + s_z$. On such a manifold, the Zeeman energy (for equal g factors) is a constant of motion and can be ignored. Taking the net conduction-electron polarization to be in the up direction, the antiferromagnetic interaction favors the down, "binding," orientation for the impurity spin. The vertex g, for $S_z = +\frac{1}{2}$, which involves impurity-conduction-electron interactions in this binding arrangement, corresponds to a state which evolves towards the ground state, while g^*, for $S_z = -\frac{1}{2}$, involves the "antibinding" configuration and is associated with a state which evolves towards an excited (triplet) state. The relative intermediate-state energies involved in the dressed vertices g and g^* are therefore different, and it is to be expected that the vertices, g and g^*, will have different values.

The strong-coupling relationship, $g = -g^*$, is easily seen to reflect impurity scattering which is potential-like. On the other hand, in the extreme weak-coupling limit g and g^* are both equal to $\frac{1}{2}\rho J$ where J is the bare exchange coupling constant, i.e., the weak-coupling limit corresponds to an equality $g = g^*$ which indicates pure exchange scattering. These two different relationships between g and g^* can be viewed as reflecting the asymptotic symmetries of the weak and strong fixed points. Between these limits neither of these symmetries is satisfied and the Kondo problem might be described as exhibiting "broken asymptotic symmetry." This does not seem to have been recognized in earlier scaling and diagram approaches which preserve the asymptotic symmetry of the weak-coupling limit.

The properties of the conduction-electron quasiparticle states near the Fermi surface ($\varepsilon < T_0$) are somewhat surprising, at least at first sight. In particular, these conduction electrons do not have any "mixing width." Usually conduction-electron states which undergo potential, or other types of scattering, acquire a width because the original momentum label is no longer a good quantum number, i.e., these scattering states are a linear combination of the original plane-wave states. This is not a real many-body relaxation width, and in particular it can be eliminated by taking the thermodynamic limit in the unconventional way described in Sec. III. However, the elimination of this width usually has a cost, namely the conduction-electron "self-energy" defined in that section is singular on an energy scale dictated by the infrared cutoff D/N. This cutoff represents the lowest energy difference between the original k state and any state with which it mixes. In the present case the cutoff is *not* D/N. It *does not* go to zero in the thermodynamic limit but rather reaches a fixed limit of the order $4\pi T_0$. This directly implies that there is at least one regularization (i.e., method of taking boundary conditions) in which there is no mixing width even when the thermodynamic limit is taken in the regular fashion. This absence of a mixing width for conduction-electron states which lie in a continuum is very unusual for impurity scattering problems.

Usually, for a scattering process to not have an associated mixing width reflects (i) that the scattering is inelastic and (ii) that there is some kind of conservation principle. For example, inelastic scattering in which the momentum is conserved does not necessarily lead to a mixing width. However, for there to be a finite range of energies for which there is no such width would require not only the conservation of momentum but also a gap in the spectrum of the object off of which the conduction

electrons scatter. The fact that similar criterion would be, in some way, satisfied within the Kondo problem, in the strong limit, is what seems surprising.

It is not difficult to understand both requirements (i) and (ii) within a singlet ground-state model. This singlet ground state might be written as

$$|S\rangle = 2^{-1/2}(|i\uparrow\rangle\,|e\downarrow\rangle - |i\downarrow\rangle\,|e\uparrow\rangle)\,, \tag{11.2}$$

where i denotes an impurity state and e the state of the conduction electron(s) which compensate the impurity. The operators S^+,S^-, and S^z, which operate only on the *impurity spin state*, do not have any matrix elements within the ground state. The presence of a gap, and the inelastic nature of the scattering, is then associated with the finite binding energy of the singlet.

In fact, the action of each of these operators on $|S\rangle$ is to generate some state of the triplet manifold, i.e.,

$$|T+\rangle \equiv |T, S_z=1\rangle = |i\uparrow\rangle\,|e\uparrow\rangle \propto S^+|S\rangle\,,$$

$$|T-\rangle \equiv |T, S_z=-1\rangle = |i\downarrow\rangle\,|e\downarrow\rangle \propto S^-|S\rangle\,,$$

while

$$|T0\rangle \equiv |T, S_z=0\rangle$$
$$= 2^{-1/2}(|i\uparrow\rangle\,|e\downarrow\rangle + |i\downarrow\rangle\,|e\uparrow\rangle) \propto S^z|S\rangle\,.$$

Clearly the effect of repeated longitudinal scattering is to take the impurity ground state $|S\rangle$ first to $|T0\rangle$, then back to $|S\rangle$, then $|T0\rangle$, and so on, alternating between the singlet and triplet. Transverse scattering takes $|S\rangle$ to $|T+\rangle$ or $|T-\rangle$. Another transverse scattering event results in a linear combination of $|S\rangle$ and $|T0\rangle$. However, it is easy to see, when both the S^+S^- and S^-S^+ paths are taken together, that the $|S\rangle$ amplitude cancels. This is equivalent to the observation that the combination of vertices TT is an effective longitudinal vertex, i.e., as usual the longitudinal diagrams, or the processes which they represent, can be taken as a skeleton set to be dressed by including the series $L + TT + TLT + \cdots$.

One then must examine the skeleton longitudinal processes. Without any impurity dressing, the LL "self-energy" is

$$(J/4N)^2 \sum_{k'} (\varepsilon - \varepsilon_{k'})^{-1}\,,$$

while adding the two-particle impurity self-energy results in

$$(J/4N)^2 \sum_{k'} [\varepsilon - \varepsilon_{k'} + \Sigma(\varepsilon - \varepsilon_{k'})]^{-1}\,.$$

Since $\Sigma(\varepsilon)$ changes sign at $\varepsilon=0$ and is odd, this sum is essentially zero. The only corrections come from band edges and imply such contributions contain a small factor of ε/D.

A "self-energy" which involves an impurity intermediate state $|S\rangle$, and which can thereby lie within $O(D/N)$ of the initial state, is necessarily of $O(L^4)$. However, it, and all higher-order similar terms, necessarily involve the above very small sum at least twice. As a result, all contributions, *except* the dressed $O(L)$ terms, are negligible. Stated another way, there are no significant scattering processes which involve an intermediate-state energy which is within $4\pi T_0$ of the ground state. This can be thought of as reflecting some special conservation principle (or selection rule) for the scaling limit.

(It might be noted that it *is* possible to have momentum conservation over a limited range even with impurity potential scattering. A suitable potential can be constructed by taking the Fourier transform of a spectrum which is zero for some finite range of momentum. For example, the potential

$$v\{\delta(x) - 2[\sin(k_0 x)/x]\} \tag{11.3}$$

reflects a spectrum in which the minimum transfer of momentum is k_0.)

The fact that in a particular regularization there is no mixing width does not imply that there are not others in which such a width does occur. (In terms of the simple potential scattering example given above, the δ function might be absorbed into the unperturbed conduction-electron energy as an energy-independent shift. In this case the second term alone *does* lead to a mixing width $\sim \pi\rho v^2$.) The inverse process, in which a mixing width is eliminated, is in fact well known and corresponds to the methods of phase-shift analysis. In this case a mixing width obtained by calculating the t matrix is converted into an energy shift of the conduction-electron states. This energy shift is the one which would be obtained if instead the reaction matrix formalism was used. In the preceding section the inverse process was used, i.e., the t matrix was obtained from the reaction matrix formulation. It is via the t matrix that the resistivity is usually calculated. Results have been given in that section.

These different possible regularizations are also important for a correct understanding of the nature of the effective interaction in the strong limit. After Anderson *et al.*,[2] Wilson,[1] and Nozières,[19] it is usually stated that the strong limit corresponds to an effective infinite exchange, i.e., a limit $J_{\text{eff}} \to \infty$. The resulting ground state is a singlet and the phase shift at the Fermi surface is $\pi/2$. Here the same results follow, i.e., there is a singlet ground state and $\delta = \pi/2$. However, the effective interaction vertices g and g^* *do not* diverge, but rather attain finite values. These two pictures are *not* inconsistent. The difference is associated, again, with the use of a reaction matrix formalism in the present work. When the effective t matrix is constructed, as in Sec. X, it is of the form

$$(1/\rho N)(4T_0/\varepsilon)/[1 - (4T_0/\varepsilon) i\pi]\,,$$

which corresponds to impurity scattering with a strength $4T_0\varepsilon$. This is indeed infinite in the strong-coupling limit $\varepsilon \to 0$. In fact, the present results are, by and large, compatible with these earlier notions.

As was noted in Sec. V, in the $U=\infty$ limit the so-called "no crossing approximation"[20] would lead to an identical scaling equation, i.e., Eq. (5.11). However, that approach is not equivalent to the present one for several reasons. Most specifically, the scaling equation would involve the energy ε rather than the field h as the variable. Because the no crossing approximation involves a mixture of longitudinal and transverse diagrams, the corresponding self-energy is not a function of only ε (or $\varepsilon + h$), and

so would not lead to (5.11) if written as a function of the field. Also, usually that approximation is formulated in terms of what is essentially a single-particle self-energy rather than the two-particle self-energy used in the present derivation of (5.11). Because of its single-particle nature it does not exhibit broken asymptotic symmetry, i.e., different strong-coupling self-energies for the "up" and "down" propagators. If the two-particle self-energy were calculated it *would* most probably lead to (5.11), but again for that quantity as a function of the energy. The strong-coupling limit would therefore correspond to $\varepsilon \to 0$. Here, in contrast, the strong limit is $h \to 0$ for the self-energy, on shell, i.e., for a finite energy. This difference is important because for $T=0$ there must be discontinuities in either the single- or two-particle self-energies at an energy corresponding to the separation between the singlet and triplet. Singular behavior *does* occur in the no crossing approximation. Here it is this singlet-to-triplet separation as a function of field which is actually calculated. Clearly, on physical grounds, with increasing fields this evolves, without singular behavior, into that between the $S_z = \pm \frac{1}{2}$ levels. When single-particle self-energies *are* calculated in the present work no attempt is made to connect them with perturbation theory and it is again the value of the (i.e., kink) self-energy on shell which is of interest. On shell, the longitudinal diagrams do not contribute and are *not* to be included. In fact, it has been shown here that the Dysonian single-particle longitudinal self-energy is not unique, indicating that any approximation which involves such diagrams in an essential way can only be correct by accident. It seem probable that it is the similarity of the results of the no crossing approximation to those derived here which accounts for the remarkable success of that method.

Within the present formalism, the following picture of the formation of the Kondo ground state emerges. As is well known, the ground state is an energetic and spin singlet. The compensating conduction electrons adjust themselves in such a way as to provide a cutoff for the logarithmic (and other) integrals of the theory. This implies that there is an unusual conservation principle in that conduction-electron states within $4\pi T_0$ of the Fermi surface only interact significantly with states outside this range. An interesting concept, which the present work illustrates, is that of "broken asymptotic symmetry." The symmetry exhibited by the renormalized weak-coupling theories (i.e., $g=g^*$) is broken in the exact solution.

It is relatively easy to generalize the present methods to the general spin problem and to the Anderson model in the magnetic, i.e., large-U, limit. The generalization to this Anderson model used the Abrikosov method for this model. Results of these calculations will be published elsewhere.

Of more interest is the prospect of applying the same methods to the lattice problems. Particularly, because of the absence of the linked cluster theorem this would appear prohibitive. However, the Abrikosov method for the Anderson lattice has been studied with some success.[21] In fact, the application of the near Fermi surface properties of the heavy-fermion problem seems relatively straightforward; this because the symmetry in the strong limit is the same as for plain potential scattering (despite the existence of the effective electron-electron interaction). With this symmetry only the combination $n_{d\uparrow}+n_{d\downarrow}=1$ appears. Because of this a separate calculation of the partition function is not needed. It is hoped that results for the lattice models, using the present methods, will be forthcoming in the near future.

ACKNOWLEDGMENTS

The author wishes to thank T. K. Lee for helpful criticism of the manuscript. This work was supported in part by a U.S. National Science Foundation (NSF) grant (No. DMR-81-20827) and, in the early stages, in part by the Swiss National Fund for Scientific Research.

APPENDIX

In this appendix are given some details of the way in which the various bubbles overlapping bubbles type of vertex corrections cancel against each other and transverse dressings of the same bubbles. Some of these cancellations will only be valid for an isotropic exchange interaction.

Even in the fourth order where these vertex corrections, etc., first occur it is prohibitive to directly derive each of the contributions to the relevant two-particle and kink self-energies. For this reason use will be made of the rules of thumb derived in the text. Also, since such fourth-order diagrams involve four integrations upon conduction-electron energies a quick method of evaluating the $\ln(h/D)$ divergences will be used. This latter method will first be illustrated by using it to evaluate the $O(J^2)$ self-energy.

The $O(J^2)$ self-energy, Fig. 3(a), on the (nominal) energy shell is

$$(J/N)^2 \sum_{k,k'} [n_{k\downarrow}(1-n_{k\uparrow})/(\varepsilon_{k\uparrow}-\varepsilon_{k'\downarrow}-h)] \; . \tag{A1}$$

If the sums are converted to integrals, this becomes

$$(\rho J)^2 \int_0^D d\varepsilon \int_{-D}^0 d\varepsilon'(\varepsilon-\varepsilon'-h)^{-1} \; . \tag{A2}$$

If then the variables of integration are changed so that $y=\varepsilon-\varepsilon'$ and if only the most divergent small y part of the integral is retained, this becomes

$$(\rho J)^2 \int_0^D dy\, y(y-h)^{-1} = (\rho J)^2 \left[D + h \int_0^D dy (y-h)^{-1} \right]$$
$$= (\rho J)^2 \{ D - h \ln[-h/(D-h)] \} \; . \tag{A3}$$

The "trick" of interest is that used to convert (A2) into the first line of (A3). When used on such logarithmic integrals it reduces the number of integrals by factor of 2. It is not difficult to include those parts of the integrals omitted in (A3); however, they are not important for the evaluation of the leading divergence and will not omitted for clarity in what follows.

Turning out to the actual omitted $O(J^4)$ contributions, it is first useful to consider together the overlapping terms

which occur in the kinked "self-energy" and which arise from the dressing of the line other than the one which carries the self-energy of interest. Specific diagrams are illustrated in Fig. 32. The partial fraction expansion sequence used here is different, but equivalent, to that suggested in Sec. IX. The sequence is tailored to keep the same vertex at the top of each diagram. The diagrams cancel against a diagram vertically below. There are many similar cancelling pairs not illustrated here. This is a very good cancellation since it is associated with the fact that $n_{d\uparrow}+n_{d\downarrow}=1$ is a constant of motion.

The remaining bare two-particle kink self-energy diagrams only have vertices on a single line. As a consequence the $O(J^4)$ kink diagrams for both the single- and two-particle propagators are the same in this order. The important omitted diagrams, involving two $O(J^2)$ self-energies and up spin, are shown in Figs. 33 and 34. Not shown is the transverse dressing of the longitudinal self-energy, i.e., diagrams similar to Figs. 33(b) and 33(c), except that the top and bottom vertices are longitudinal. These give zero by symmetry.

The overlapping transverse on transverse diagram [Fig. 33(a)] corresponds to an integral:

$$\int d\varepsilon\,\varepsilon \int d\varepsilon'\,\varepsilon'(\varepsilon'-h)^{-1}(\varepsilon-\varepsilon')^{-1}(\varepsilon-h)^{-1}\,, \qquad \text{(A4)}$$

and is also zero by symmetry (make the interchange of variables $\varepsilon\leftrightarrow\varepsilon'$).

The overlapping transverse with longitudinal diagrams of Fig. 34 correspond to an integral:

$$\int d\varepsilon\,\varepsilon \int d\varepsilon'\,\varepsilon'(-\varepsilon)^{-1}(\varepsilon'-\varepsilon-h)^{-1}(\varepsilon'-h)^{-1}$$

$$= \int d\varepsilon \int d\varepsilon'\,\varepsilon'(\varepsilon'-\varepsilon-h)^{-1}(\varepsilon'-h)^{-1}\,, \qquad \text{(A5)}$$

which can be integrated to give

$$(h/2)\ln^2(h/D)\,. \qquad \text{(A6)}$$

However, the two diagrams in this figure have the same central denominator, but with the opposite sign, and cancel against each other.

Last is the real "cross" vertex correction such as that shown in Fig. 35(a). There are similar *TLTL* corrections. Such a vertex correction generates a total of six two-particle self-energies. The *TTTT* contributions correspond to the diagrams in Fig. 35(b). Those diagrams vertically above each other have the same (leading order) value. The kink diagrams obtained from these simply corresponds to putting them on their nominal energy shells, i.e., with the external frequency $i\omega_0=h$. Explicitly, the sum of the first two inequivalent diagrams shown in the top line of Fig. 35(b) is

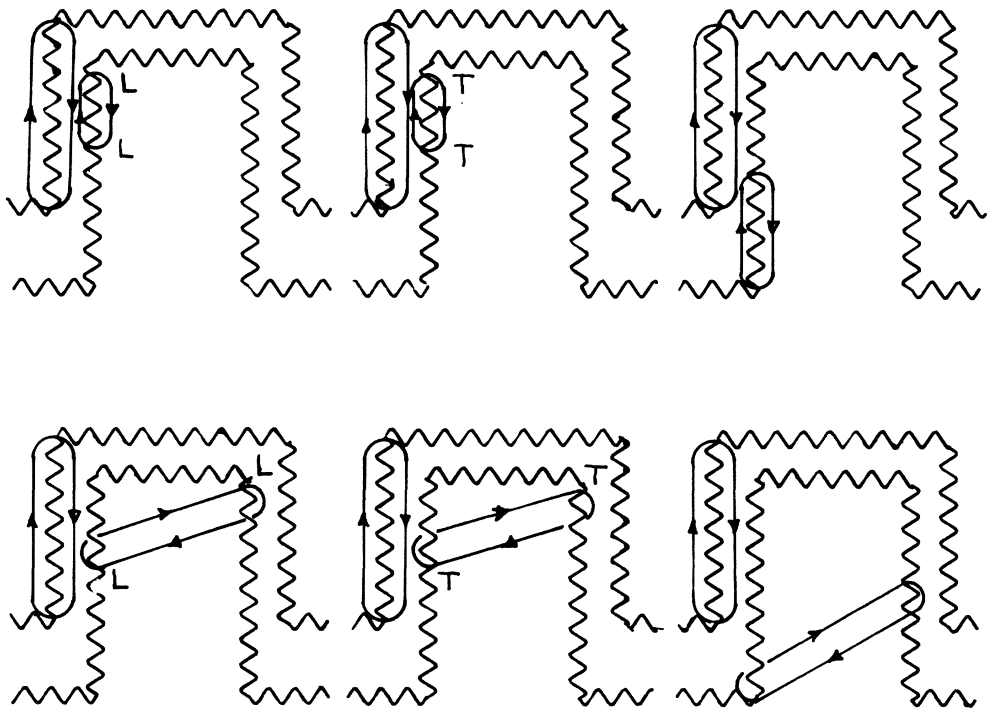

FIG. 32. Selection of overlapping diagrams which involve both lines of the two-particle propagator. The left two pairs have the vertices of the dressing labeled as longitudinal, L, or transverse, T. The overlapping vertex correction to the right can have any labels.

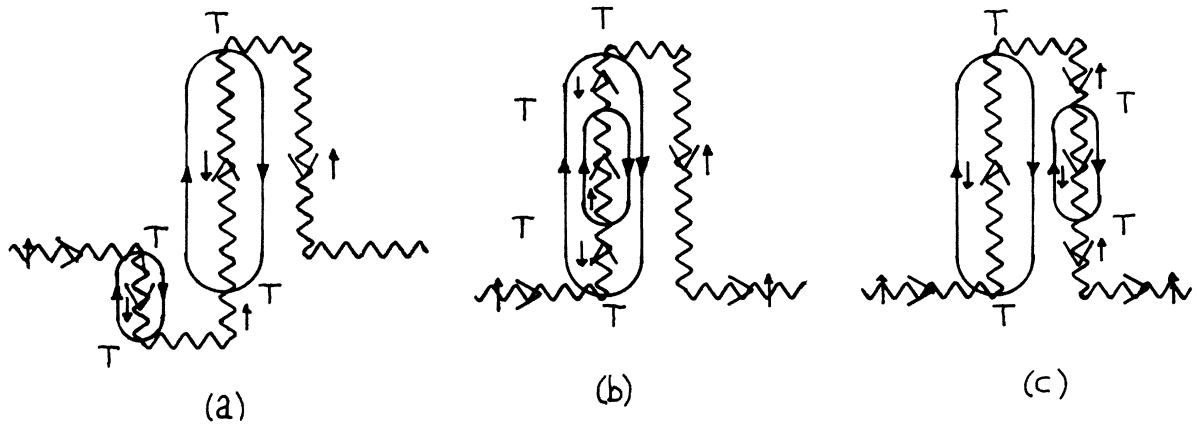

FIG. 33. On the left is a overlapping vertex correction, while on the right is a similar dressing. The middle corresponds to a direct dressing.

$$\int d\varepsilon\,\varepsilon \int d\varepsilon'\,\varepsilon'(\varepsilon-h)^{-1}[2h-(\varepsilon-\varepsilon')]^{-1}(\varepsilon'+h)^{-1}+\int d\varepsilon\,\varepsilon \int d\varepsilon'\,\varepsilon'(\varepsilon-h)^{-2}[2h-(\varepsilon-\varepsilon')]^{-1}$$
$$=\int d\varepsilon'\,\varepsilon'(\varepsilon'+h)^{-1}\int d\varepsilon\,\varepsilon(\varepsilon-h)^{-2}\,. \quad \text{(A7)}$$

Evaluating the integral gives

$$-h\ln^2(h/D)\,. \quad \text{(A8)}$$

However, the last term on the top line or the diagram gives

$$\int d\varepsilon\,\varepsilon \int d\varepsilon'\,\varepsilon'(\varepsilon-h)^{-2}(\varepsilon-\varepsilon')^{-1}\,, \quad \text{(A9)}$$

and this cancels (A8). The same null result follows for the *TLTL* vertex correction.

To complete the discussion of omitted diagrams, it is necessary to consider the relevant dressing for the included diagrams. The question at issue is the evaluation of the effective cutoff $Z=\Sigma-h$ first defined in the Introduction. This arises from the differentiation of the logarithmic integrals, Eq. (5.9), i.e., $d/dh\,I^{\pm}=Z^{-1}=(\Sigma-h)^{-1}$. It is not difficult to appreciate that the quantity $\Sigma-h$ involves the two-particle self-energy of the transverse susceptibility evaluated at zero external frequency. (Note, in particular, that the effective cutoff corresponds to the zero-energy limit of each conduction-electron integration. As a result the conduction electrons do not contribute to Z, leaving only the impurity self-energy. Lastly, there is no frequency argument to a kink self-energy, so the relevant impurity dressing corresponds to the zero frequency rather than, say, the energy shell value.) It is trivial that the transverse dressing is zero for zero external frequency. Thus as stated in the body of the text, only the longitudinal dressing contributes to the cutoff in the scaling equation. The same conclusion remains valid when one constructs the scaling equation for this longitudinal dressing.

One can also check that there are no omitted next to leading corrections to this effective cutoff, Z. Now there are real vertex corrections such as in Fig. 1(a), with all the impurity spin labels the same, and also *LLLL* overlapping terms of the structure of Fig. 9(a). In total there are four

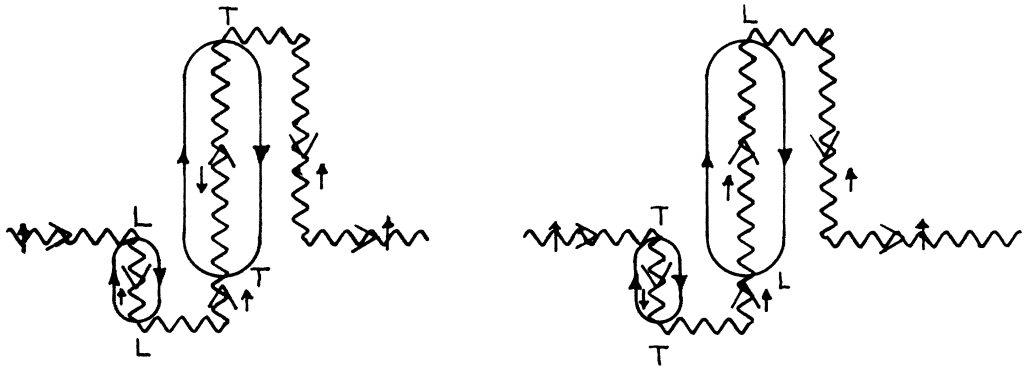

FIG. 34. Shown are the two overlapping *LTLT* and *TLTL* diagrams.

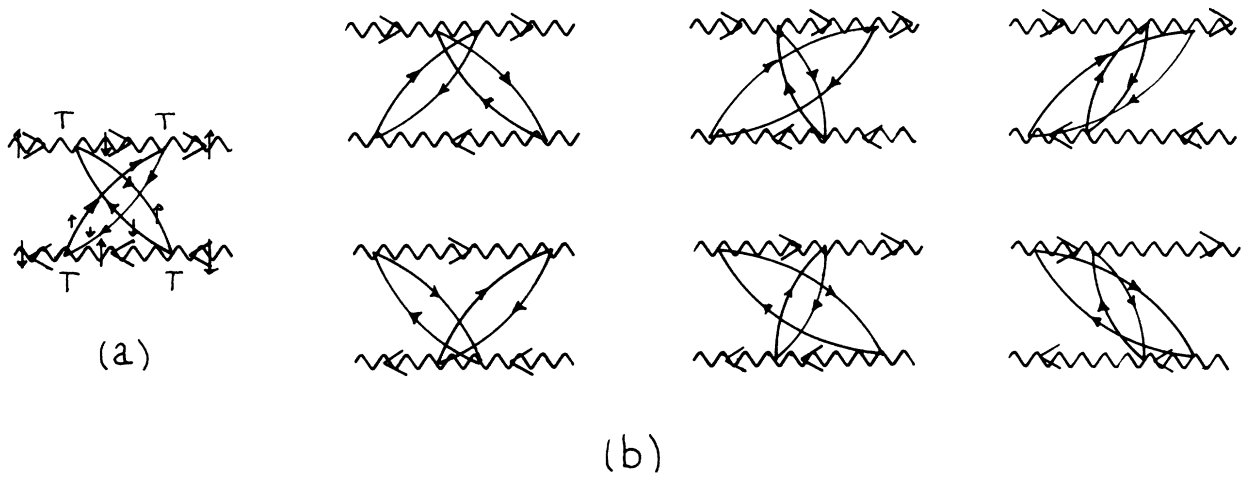

FIG. 35. (a) The $O(J^4)$, *TTTT*, vertex correction. (b) The four two-particle self-energies associated with the four possible time orderings of the vertices.

such contributions, each of which is equivalent to an integral:

$$\int d\varepsilon\,\varepsilon \int d\varepsilon'\,\varepsilon'(\varepsilon+h)^{-1}[(\varepsilon+\varepsilon'+h)]^{-1}(\varepsilon'+h)^{-1}\,, \quad \text{(A10)}$$

and gives an $h\ln^2 h$ contribution. This cancels against the four *LTTL* dressings of the structure of either Fig. 9(b) or the direct dressing corresponding to the structure of Fig. 17(b). The corresponding integrals are, e.g.,

$$\int d\varepsilon\,\varepsilon \int d\varepsilon'\,\varepsilon'(\varepsilon-h)^{-2}(\varepsilon-\varepsilon')^{-1} = -\int d\varepsilon\,\varepsilon \int d\varepsilon'\,\varepsilon'(\varepsilon-h)^{-2}(\varepsilon'-h)^{-1} + \int d\varepsilon\,\varepsilon \int d\varepsilon'\,\varepsilon'(\varepsilon-h)^{-1}(\varepsilon-\varepsilon')^{-1}(\varepsilon-\varepsilon')^{-1}(\varepsilon'-h)^{-1}\,. \quad \text{(A11)}$$

All *TLTL* vertex corrections cancel in pairs.

The evaluation of the effective cutoff Z illustrates the resolution of an apparent contradiction. In the Introduction it was noted that the next to leading order should be small as compared to the leading order by a factor of ρJ in the scaling limit. Yet it is necessary to include longitudinal dressing in the construction of the scaling theory. The above discussion illustrates why this is the case. In order that the scaling equation in general, and the cutoff Z in particular, be accurate to leading order it is necessary to evaluate these diagrams which in the asymptotic series are of next to leading order. It is, of course, such diagrams which lead to the factor $|\rho J|^{1/2}$ in the energy scale.

Next to leading order diagrams which do not contribute to Z *can* be to taken to be small. In particular, the transverse dressings of the transverse self-energy shown in Figs. 33(b) and 33(c) both give the same leading terms, e.g., corresponding to Fig. 33(c) is a integral:

$$\int d\varepsilon\,\varepsilon \int d\varepsilon'\,\varepsilon'(\varepsilon-h)^{-2}(\varepsilon-\varepsilon')^{-1} = -\int d\varepsilon\,\varepsilon \int d\varepsilon'\,\varepsilon'(\varepsilon-h)^{-2}(\varepsilon'-h)^{-1} + \int d\varepsilon\,\varepsilon \int d\varepsilon'\,\varepsilon'(\varepsilon-h)^{-1}(\varepsilon-\varepsilon')^{-1}(\varepsilon'-h)^{-1}\,, \quad \text{(A12)}$$

and *is* to next to leading order but is not needed in the scaling limit.

[1]K. G. Wilson, Rev. Mod. Phys. **47**, 773 (1975).
[2]P. W. Anderson, G. Yuval, and D. R. Hamann, Solid State Commun. **8**, 1033 (1970); Phys. Rev. B **1**, 4664 (1970); P. W. Anderson and G. Yuval, Phys. Rev. Lett. **23**, 89 (1969); J. Phys. C **4**, 607 (1971); *Magnetism Volume V*, edited by H. Suhl (New York, Academic, 1973), p. 217.
[3]See A. M. Tsvelick and P. B. Wiegman, Adv. Phys. **32**, 453 (1983); N. Andrei, K. Furuya, and J. H. Lowenstein, Rev. Mod. Phys. **55**, 331 (1983).
[4]See, e.g., F. D. W. Haldane, Phys. Rev. Lett. **40**, 416 (1978); P. Coleman, Phys. Rev. B **29**, 3035 (1984); K. Yamada, Prog. Theor. Phys. **53**, 970 (1975); S. Inagaki, *ibid.* **62**, 1441 (1979).
[5]P. Coleman, Phys. Rev. B **29**, 3035 (1984).
[6]S. E. Barnes, J. Phys. F **6**, 115 (1976); **6**, 1375 (1976); **7**, 2637 (1977); and see also, Adv. Phys. **30**, 801 (1980), and references therein.
[7]See S. E. Barnes, J. Phys. F **7**, 2637 (1977).
[8]T. Holstein, Ann. Phys. (N.Y.) **29**, 410 (1964).
[9]S. E. Barnes and J. Zitkova-Wilcox, Phys. Rev. B **7**, 2163 (1973).
[10]A. A. Abrikosov and A. A. Migdal, J. Low Temp. Phys. **3**, 519 (1970).

[11]A. A. Abrikosov, Physica **2**, 5 (1965).
[12]G. D. Mahan, *Many-Particle Physics* (Plenum, New York, 1981).
[13]W. Kohn and J. M. Luttinger, Phys. Rev. **108**, 590 (1957).
[14]P. W. Anderson, Phys. Rev. **124**, 40 (1961).
[15]S. E. Barnes, J. Phys. F **6**, 1713 (1970).
[16]R. Orbach and H. J. Spencer, Phys. Rev. **179**, 690 (1969).
[17]D. C. Langreth and J. W. Wilkins, Phys. Rev. B **6**, 3189 (1972).
[18]M. Fowler and A. Zawadowski, Solid State Commun. **9**, 471 (1971).
[19]A. Nozières, J. Low. Temp. Phys. **17**, 31 (1974).
[20]See F. C. Zhang and T. K. Lee, Phys. Rev. B **28**, 33 (1983); D. L. Cox, N. E. Bickers, and J. W. Wilkins, Bull. Am. Phys. Soc. **30**, 457 (1984); H. Keiter and G. Morandi, Phys. Rep. **109**, 227 (1984); S. Inagaki, Prog. Theor. Phys. **62**, 1441 (1979).
[21]S. E. Barnes, Bull. Am. Phys. Soc. **26**, 335 (1981).